npj | biosensing

Review

https://doi.org/10.1038/s44328-026-00109-7

Materials and microsystems for stable and high-efficiency brain-computer interfaces in signal recording

Check for updates

Qi Chen[1,2,3,7], Ningge Huang[1,2,4,7], Chuanjie Tong[5,7], Pengchuan Liu[1,2,4], Shaojun Que[1,2], Huize Xue[1,2] ✉, Xiao Xiao[1,3] ✉ & Enming Song[1,2,4,6] ✉

Brain–computer interfaces enable high-resolution neural recording, yet chronic performance is constrained by interacting factors across materials, electrode and array architectures, and microsystem integration. This review examines how these cross-level design layers collectively shape recording stability, efficiency, and scalability. We summarize representative degradation patterns, strategies for improving long-term performance, and recent advances in integrated systems, and outline design principles for clinically scalable and reliable neural interfaces.

Brain–computer interfaces (BCIs) rely on neural recording as the foundation for decoding brain activity and enabling interaction with external devices. High-quality neural recording underpins a wide range of clinical and experimental applications, including motor intention decoding, assistive communication, rehabilitation, and closed-loop neuromodulation in patients with spinal cord injury, amyotrophic lateral sclerosis, and stroke[1–12]. While short-term studies have demonstrated the feasibility of acquiring neural signals, achieving stable, long-term, and scalable neural recording remains a central challenge as BCIs move toward chronic and clinical use[13–15].

During chronic implantation, the electrode-neural interface undergoes persistent biological and physical changes, such as inflammation and glial scar formation, which increase interface impedance and degrade signal quality by reducing amplitude, increasing noise, and diminishing recording selectivity. Importantly, chronic recording performance is not determined by any single design factor, but arises from the combined effects of electrode materials and structures, active devices, array architecture, and microsystem integration. As a result, optimizing individual components alone is insufficient to meet the stability and efficiency required for long-term clinical use, making chronic neural recording a fundamentally cross-level, system-level challenge.

In electrode-neural interface design, materials and structures jointly define the mechanical and electrochemical coupling with neural tissue, thereby constraining initial signal quality, interface impedance, and biocompatibility[15,16]. Electrode materials primarily govern electrochemical stability and tissue responses, while electrode structure determines spatial resolution and recording stability through geometric design and mechanical compliance under chronic implantation. Accordingly, these material and structural choices bound the achievable impedance, effective recording volume, and long-term interface stability[17–20]; In *Electrodes in BCI Systems*, we review representative electrode materials and architectures with a focus on their implications for stable chronic neural recording.

However, passive electrode-neural interfaces alone are insufficient to function as high-fidelity signal transducers, particularly under chronic implantation, where stable detection of low-amplitude neural activity remains challenging. To overcome this fundamental limitation, active devices are required to perform in situ amplification, modulation, and transmission of neural signals, thereby preserving recording accuracy and information integrity[21,22]. Recent advances in low-noise amplifiers, signal transmission schemes, and energy-efficient microelectronics have substantially improved system sensitivity and long-term stability[23,24]; *Microsystem Architectures for Neural Signal Recording* focuses on active device architectures and signal conduction strategies, highlighting how they address the physical and engineering limitations of passive recording to enable efficient and reliable neural signal acquisition.

As neural recording evolves from single-channel measurements to multichannel acquisition, array-level design becomes critical for achieving stable, long-term recording at the cortical scale. Even with advanced active devices, isolated recording sites are insufficient to capture distributed neural activity across large brain areas, motivating the development of high-density, large-area electrode arrays. While increasing array density and size expands spatial coverage, it also influences tissue interactions, system

[1]Institute of Optoelectronics & College of Future Information Technology, Shanghai Frontiers Science Research Base of Intelligent Optoelectronics and Perception, Institute of Science and Technology for Brain-Inspired Intelligence, College of Smart Materials and Future Energy, Fudan University, Shanghai, China. [2]International Institute for Intelligent Nanorobots and Nanosystems, Brain-Computer Interface Research, Fudan University, Shanghai, China. [3]Behavioral and Cognitive Neuroscience Center, Fudan University, Shanghai, China. [4]Yiwu Research Institute of Fudan University, Yiwu, China. [5]Integrated Circuits and Microelectronics Engineering, Anhui University, Hefei, China. [6]State Key Laboratory of Integrated Chips and Systems, MOE Frontiers Center for Brain Science, Fudan University, Shanghai, China. [7]These authors contributed equally: Qi Chen, Ningge Huang, Chuanjie Tong. ✉e-mail: huize_xue@fudan.edu.cn; xiaoxiao@fudan.edu.cn; sem@fudan.edu.cn

stability, and long-term signal quality through array-level factors such as channel count, power distribution, interconnect routing, mechanical compliance, and data transmission[25–27]; *Design Strategies of Electrode Arrays for High-Resolution Neural Recording* reviews representative large-scale array implementations and examines how array architectures are engineered to support stable, long-term neural recording.

Evidence from animal models shows that long-term neural recording performance ultimately depends on coordinated design across materials, device architecture, array configuration, and microsystem integration under realistic implantation conditions. Chronic studies in rodents and non-human primates consistently demonstrate that mismatches across these levels lead to signal degradation, whereas integrated design strategies can support stable recordings over extended periods. *Experimental Demonstrations and Translational Studies* summarizes in vivo validation results and identify the cross-level factors that determine the reliability of chronic neural recording. Finally, *Frontier Directions in BCI Devices and Microsystems* discusses emerging challenges and design principles for next-generation, clinically scalable BCI recording systems.

Existing reviews often discuss performance improvements at a single level, while providing limited systematic analysis of how different levels influence overall recording performance under long-term operating conditions[28–32]. In contrast, this review takes long-term neural recording as the central problem and systematically analyzes design choices across materials, active devices, array architectures, and microsystem integration, clarifying their decisive roles in recording stability, efficiency, and scalability under chronic implantation.

Electrodes in BCI Systems

BCIs represent an emerging neurotechnology that establishes a direct communication pathway between the human nervous system and external devices. Their overarching goal is to convert neural activity into actionable outputs for fundamental neuroscience, neural repair, and clinical rehabilitation. Neural signals originate from distributed cortical and subcortical circuits and can be accessed through non-invasive, semi-invasive, or invasive modalities, ranging from scalp electroencephalography (EEG) to electrocorticography (ECoG) and penetrating intracranial electrodes. Following acquisition, neural signals are subjected to signal conditioning and decoding processes (including amplification, filtering, feature extraction, and classification) to generate control commands for external systems. The capability of efficient neural signal acquisition is essential for clinical translation. As illustrated in Fig. 1a, closed-loop or bidirectional BCI systems incorporate feedback pathways that record neural activity from brain regions associated with motor, visual, auditory, and language functions. The acquired signals are subsequently processed and decoded into control commands to drive external devices or assistive systems, enabling adaptive interactions between neural circuits and artificial devices. Based on their functional objectives and therapeutic strategies, closed-loop BCI systems are primarily applied in three domains: (1) disease treatment (e.g., epilepsy, Parkinson's disease, essential tremor, and major depressive disorder), (2) functional rehabilitation (e.g., stroke and spinal cord injury), and (3) health monitoring and diagnosis (e.g., Alzheimer's disease and sleep disorders; see *Human Clinical Studies* for details)[33–41]. Within such systems, electrodes constitute the critical physical interface between the brain and external electronics, fundamentally determining the type, quality, and long-term reliability of accessible neural information. To support stable closed-loop operation under chronic implantation, BCI electrodes must simultaneously achieve high signal fidelity, long-term recording stability, high channel density, and mechanical and biological compatibility with neural tissue.

At the material-tissue interface, recording quality determined by the electrical conduction, electrochemical behavior, and interfacial impedance of electrode materials, which govern amplitude attenuation, noise, and spectral fidelity. In parallel, the structural scale, geometry, and spatial layout of electrodes further constrain the effective recording volume, spatial selectivity, and the ability to resolve weak, localized neural activity. Together, material and structural classifications provide a physical framework for comparing neural interface performance.

Geometrical architectures of BCIs electrodes

The classification of neural electrodes by structural dimensionality arises from the spatial organization of the brain and the distribution of neural signals. Different brain regions impose distinct requirements on recording depth, coverage area, and spatial resolution, leading to the development of one-dimensional (1D), two-dimensional (2D), and three-dimensional (3D) electrode architectures, with representative examples summarized in Table 1 and Fig. 1b. 1D electrodes consist of recording sites arranged along a single axis, typically enabling access to deep brain structures through penetrating probes. 2D electrodes distribute recording sites across planar surfaces and are widely used for cortical surface mapping. In contrast, 3D electrode architectures achieve volumetric sampling by stacking multiple layers or arranging probes in three-dimensional configurations, allowing simultaneous interrogation of distributed neural networks. Thus, electrode dimensionality fundamentally reflects the need to spatially match recording architectures with the anatomical and functional organization of the brain.

1D Electrodes. Early deep-brain electrodes were predominantly based on metal microwire structures, developed to overcome the fragility and high impedance of glass microelectrodes originally designed for intracellular recordings[42]. Owing to their mechanical robustness and favorable electrochemical properties, tungsten microwires became a standard platform for extracellular single-unit recording, enabling high signal-to-noise ratios through micrometer-scale tips and localized recording geometries[43].To improve the discrimination of individual neurons within multiunit activity, multi-contact configurations such as stereotrodes and tetrodes were introduced. By exploiting amplitude and waveform differences across closely spaced channels, these designs significantly enhanced single-unit isolation, as demonstrated by the stereotrode technique[44] and the tetrode architecture developed by O'Keefe and Recce[45]. Despite their effectiveness for acute and short-term recordings, metal microwire- and tetrode-based probes exhibit intrinsic limitations for chronic neural recording. Restricted channel scalability, susceptibility to corrosion in biological environments, and limited long-term biocompatibility constrain their ability to support stable, high-density recordings over extended implantation periods. These limitations ultimately motivated the transition toward microfabricated and integrated electrode platforms for scalable and long-term neural recording.

With the development of microelectromechanical systems (MEMS) technology, silicon-based neural probes have progressively emerged as an important alternative to metal microwires. These probes typically integrate metal electrode arrays on a silicon substrate, with electrical insulation and channel isolation achieved through dielectric layers such as SiO_2. This architecture significantly reduces parasitic capacitance and inter-channel crosstalk noise. Wise et al. pioneered the development of silicon-based neural probes using integrated circuit fabrication techniques, integrating metal electrode arrays on a 50-μm-thick silicon substrate. The probes featured tip diameters of ≥2 μm and inter-electrode spacings of 10–20 μm[46]. Building on this work, Drake et al. reduced the silicon substrate thickness to 15 μm and narrowed the probe tip width to 20 μm. By adopting midline and diamond-shaped electrode layouts with minimum spacings of 30–42 μm, this design enabled the separation of 2–3 neuronal units per recording site, achieved a neural recording range of approximately 180 μm, and produced signal amplitudes as high as 675 μV. The study also provided systematic quantitative evaluations of in vivo recording performance and long-term stability[47]. Compared with metal microwires, silicon-based probes offer higher channel densities and more precise recording capabilities[48].

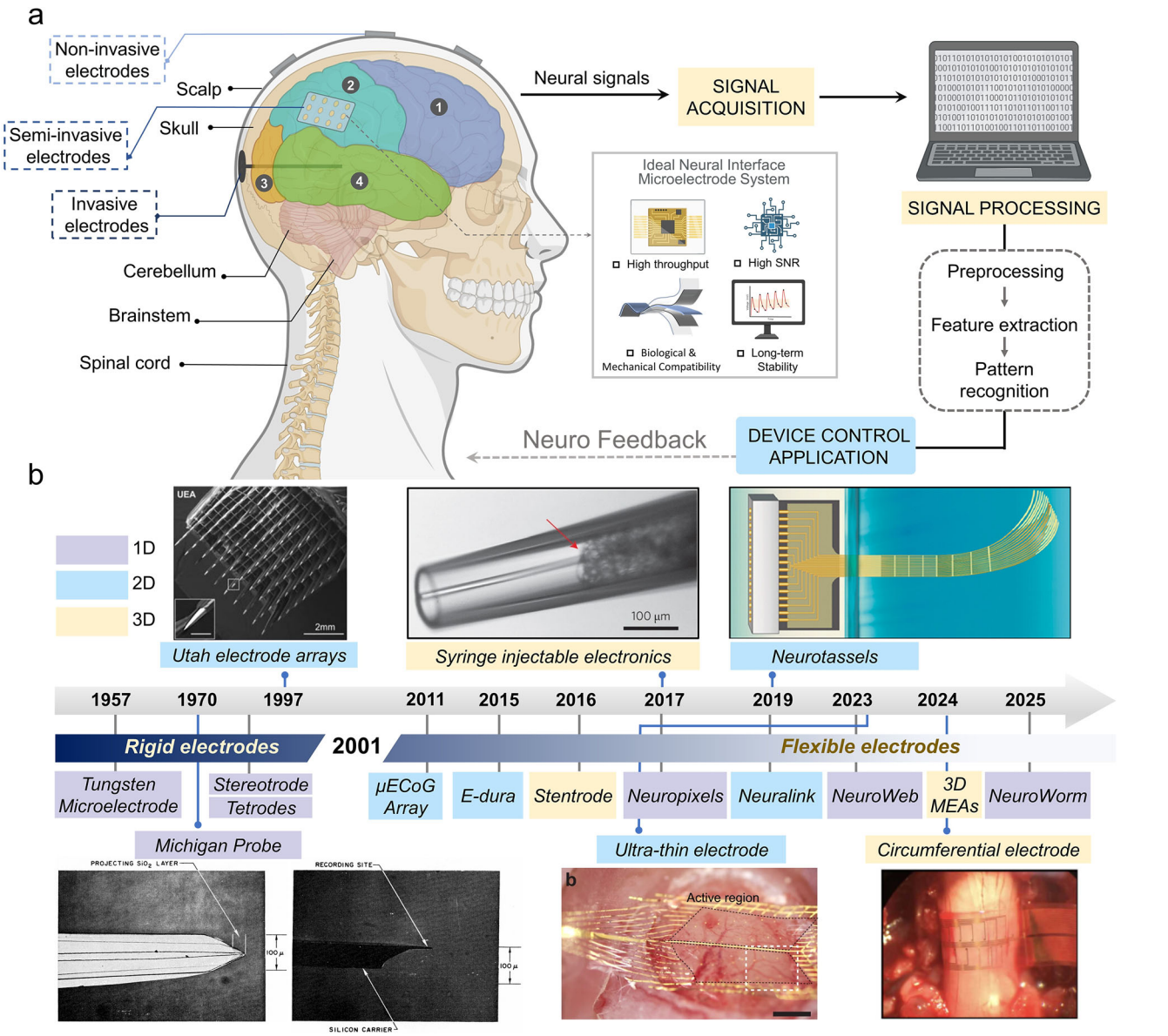

Fig. 1 | A schematic of a brain-computer interface (BCI) technology workflow and timeline of the development of BCI electrodes around the world. **a** Illustration of BCI technology workflow, created with BioRender (https://biorender.com). **b** Timeline charts of the evolution of neural electrodes, splitting into rigid electrodes (Michigan Probe[46], Utah electrode arrays[241], etc.) and flexible electrodes (post-2001, e.g., Neurotassels[251], Injectable electronics[94], Ultra-thin electrode[274], Circumferential electrode[275], etc.), showing technological shifts in neural interfacing[94] Copyright 1970, IEEE[241]. Copyright 2020, American Chemical Society[251]. Copyright 2019, AAAS[84] Copyright 2015, Springer Nature Ltd[274]. Copyright 2023, Springer Nature Ltd[275]. Copyright 2024, AAAS. Different colors on the panel represent the three dimensions of the neural interface. Details are provided in Table 1.

In recent years, high-density silicon probes fabricated using Complementary metal-oxide-semiconductor (CMOS) technology have represented a major direction in the development of invasive neural electrode systems. Probes exemplified by the Neuropixels platform achieve ultrahigh channel densities with low-noise signal acquisition by integrating on-chip amplification, multiplexing, and analog-to-digital conversion. The first-generation Neuropixels probe integrated 960 low-impedance (149 ± 6 kΩ) TiN recording sites onto a single shank measuring 10 mm × 70 μm × 20 μm[49]. Neuropixels 2.0 further advanced this architecture through miniaturization and modularity, featuring dual-shank designs with a total head-mounted weight of 1.1 g and supporting multi-probe configurations comprising up to four probes and 5120 recording sites[49,50]. Despite these capabilities, the high elastic modulus of silicon leads to mechanical stress concentration and chronic inflammatory responses following long-term implantation, which limits the suitability of silicon probes for chronic neural interfaces. This challenge has emerged as a critical bottleneck in the further development of invasive neural electrode technologies.

To fundamentally mitigate chronic tissue responses induced by rigid electrode structures, research has progressively shifted toward flexible polymer-based material systems. Flexible electrodes based on polyimide (PI) improve the mechanical compliance of the electrode-brain interface by substantially reducing bending stiffness. Rousche et al. developed a PI-based flexible neural electrode featuring an ultrathin substrate (<20 μm, elastic modulus ~2.8 GPa), a width of 160 μm, a buckling force of 0.003 oz, and an in vivo impedance of approximately 190 kΩ[51]. By incorporating bioactive micro perforation structures, the device enabled deep longitudinal implantation while maintaining flexibility, thereby significantly alleviating localized immune responses. Owing to their enhanced conformability to brain tissue, flexible electrodes reduce immune reactions and improve long-term recording stability. However, the low stiffness of flexible structures

Table 1 | Classification and properties of neural interface electrodes

BCI Type		Year	Number of electrodes	Spacing (mm)	Coverage	Recording mechanism	Subject	Lifetime (days)	Ref.
1D	Rigid	1970	/	0.01–0.02	15 μm^2;	Passive	Cat	/	46
1D	Rigid	1988	8	0.03–0.2	0.08 × 0.015 mm^2	Passive	Rat	12	228
2D	Flexible	2000	4–400	PVC:0.635 mm; FPC:0.1 mm	12.7 mm × 12.7 mm	Passive	Guinea pig	/	229
1D	Rigid	2003	10	5.5	50 mm	Passive	Human	7	230
2D	Flexible	2004	91	4	24 mm × 48 mm	Passive	Human facial muscles	/	231
1D	Rigid	2004	5–10	2	/	Passive	Human	180	232
1D	Flexible	2007	16	0.1	thickness = 0.015 mm	Passive	Mouse	60	233
1D	Rigid	2007	4	0.5/1.5	10.5 mm	Active	Human	/	234
1D	Flexible	2009	4	/	1mm^2	Active	In vitro	30	235
2D	Rigid	2010	288	0.8	14.4 mm × 12.8 mm	Active	Pig	/	236
1D	Rigid	2013	16	/	diameter = 0.026 m	Passive	Zebra Finch	107	237
1D	Rigid	2014	1-3	1	length = 0.1 mm	Passive	Mouse	7	238,239
3D	Flexible	2015	16	/	/	Passive/Active	Mouse	/	240
2D	Flexible	2018	3072	0.05	23 × 18.5 × 2 mm^3	Passive	Rat	/	78
3D	Flexible	2019	16–1024	/	diameter = 0.055–0.1	Passive	Mouse	42	76
3D	Rigid	2020	100	0.4	4 mm × 4 mm	Passive/Active	goat heart	/	241
3D	/	2021	12	0.07	12.5 × 16 × 8mm^3	Active	Rat	/	242
3D	Flexible	2021	33	0.5	0.02 × 0.02 × 1.5 mm^3	Active	Rat	/	93
1D	Flexible	2022	128	0.065	0.0025 mm	Active	Mouse	/	243
3D	Flexible	2022	16	/	diameter = 0.04 mm	Active	Rat	/	244
3D	Flexible	2024	36	1 or 2	0.8 × 1.5 × 1.0 mm^3	Active	ex vivo muscle	/	245
1D	Flexible	2025	16	0.1	thickness = 0.015 mm	Active	Rat	/	246
1D/2D	Flexible	2023	128	/	0.15 × 280 mm^2	Active	Rat, Human	/	53
2D	Flexible	2023	90	0.05–0.08	thickness = 100 nm	Active	Mouse	/	77
2D	Flexible	2024	32	/	0.1 mm × 0.1 mm	Passive	Rat	42	79
2D	Flexible	2024	256	0.5	2.3 × 0.3 mm^2	Active	Rat	/	247
2D/3D	Ultra-flexible	2024	1024	/	1000/mm^3	Active	Rat	Multiple days	145
3D	Flexible	2024	64 (Scalable up to 128)	0.005	/	Active	Rat	/	248
3D	Rigid	2024	128	0.1	100 mm^2	Active	Mouse	140	249
1D	Rigid	2024	384	0.02	0.07 × 0.02 × 10 mm^3	Active	Rat	/	49
1D	Rigid	2025	768	0.032	10 × 0.07 × 0.024 mm^3	Active	Mouse	168	250
1D	Rigid	2025	1024	0.025	10–90 mm	Active	Mouse	735	201

introduces new engineering challenges, particularly probe buckling and trajectory deviation during implantation. To address these limitations, "temporary stiffening" strategies have been developed to stabilize flexible probes during insertion. Felix et al. temporarily bonded flexible PI probes (elastic modulus 2–4 GPa) to silicon stiffeners (elastic modulus ~200 GPa, thickness 20–100 μm) using a dissolvable polyethylene glycol (PEG) adhesive. The probe-stiffener assembly enabled precise implantation through microfluidic guidance, after which the stiffener was removed within 15 min, resulting in a positional displacement of only 28 ± 9 μm. This strategy effectively overcomes the implantation challenges associated with flexible probes longer than 3 mm and achieves a practical balance between compliant materials and robust engineering design[52].

Building on these advances, flexible μSEEG probes fabricated using MEMS and display-panel manufacturing processes have been developed to address the demands of implantation depth and scale required for human applications. These electrodes employ ultrathin flexible substrates that preserve the ability to access deep brain regions while integrating multi-channel, microscale recording sites. Representative μSEEG probes feature a thickness of approximately 15 μm, a width of 1.2 mm, and lengths of up to 28 cm, supporting up to 128 recording channels with contact diameters of 30 μm (Pt nanorods, PtNR) or 20 μm (PEDOT: PSS), and an inter-site spacing of 60 μm. The probes can be implanted using guidewires and are capable of recording local field potentials (LFPs), current source density, and single-unit activity in both acute and chronic experimental settings. Compared with conventional clinical sEEG electrodes, which typically operate at millimeter spatial scales with 8-16 channels, μSEEG probes offer substantial advantages in spatial resolution, channel scalability, and manufacturing cost. Moreover, they avoid the structural fragility associated with high-density silicon probes, providing a practically viable engineering pathway for high-resolution deep-brain recording and precise neuromodulation in human applications[53].

Overall, the development of one-dimensional penetrating electrodes reflects a progressive rebalancing of competing constraints imposed by long-term neural recording. Early microwire- and tetrode-based probes prioritized high signal fidelity and single-unit discrimination, but were inherently limited in channel scalability and chronic stability. Silicon-based

probes enabled substantial gains in recording density and system-level integration, yet their mechanical rigidity introduced tissue responses that constrained long-term performance. More recent flexible and hybrid designs aim to restore mechanical compliance at the electrode-tissue interface, while introducing new challenges in implantation control and system robustness. Together, these advances illustrate that stable, high-density neural recording cannot be achieved through isolated improvements in materials or fabrication alone, but requires coordinated optimization across material properties, structural design, and system integration.

2D Electrodes. By extending neural recording from discrete points to continuous cortical surfaces, 2D electrodes fundamentally amplify the challenge of maintaining stable, long-term signal acquisition. Their design is therefore dictated less by geometric considerations than by recording constraints associated with spatial scaling, interfacial stability, and system-level scalability.

Clinical ECoG grid electrodes represent the most mature and widely adopted form of 2D neural interfaces and are routinely used for epileptogenic zone localization[54] and functional cortical mapping[55–62]. Conventional clinical ECoG electrodes typically employ thick-film constructions with individual contact diameters of approximately 2 mm, arranged in array formats such as 4×4 or 8×8, covering areas of 16–64 cm^2. While these electrodes enable large-area cortical coverage, their spatial resolution is inherently limited[63]. To improve spatial resolution while preserving coverage area, high-density ECoG arrays have been developed, featuring channel counts ranging from 256 to 1024, interelectrode spacings of approximately 500 μm, and coverage areas exceeding 10 cm^2[2,64–70]. Owing to their flexibility and favorable bending compliance, these surface arrays conform more closely to the cortical surface, reducing chronic interfacial responses and improving long-term recording stability.

To further reduce mechanical loading and improve tissue compatibility, ultrathin flexible surface arrays have emerged as an important research direction. One representative example is a polyimide electrode grid supported by a silk fibroin substrate, featuring thicknesses of 2.5–7 μm and trace widths of 250 μm. Such electrodes can spontaneously conform to the cortical surface via capillary forces, with a critical thickness as low as 4.9 μm. In experiments conducted on the feline visual cortex, these arrays exhibited high signal quality, with an average RMS amplitude ratio of 5.7 ± 3.0, as well as strong spatial consistency across recording sites. This approach provides a programmable, biodegradable, and biocompatible strategy for achieving high-resolution neural interfaces[71].

2D architectures are not restricted to cortical surface interfaces; some array designs extend along the depth axis to enable simultaneous recording from subcortical and even deep brain regions. As 2D structures expand into the third dimension, mechanical modulus mismatch becomes a primary limiting factor. Conventional deep 2D arrays are predominantly fabricated from high-stiffness materials such as silicon, whose Young's modulus (>50 GPa) is orders of magnitude higher than that of brain tissue (~1–10 kPa). This severe mismatch readily induces chronic tissue responses and leads to signal degradation over time. Representative early implementations include the microelectrode array (MEA) reported by Thomas et al., which comprised 30 electrodes with tip dimensions of approximately 7 μm distributed over a 0.5 mm × 1 mm area[72]. Gross et al. developed a glass-based electrode array consisting of 36 gold traces (12 μm wide and 2 μm thick). Following UV laser ablation to create ~10 μm openings, the electrodes exhibited impedances of 2-4 MΩ and enabled simultaneous in vitro recording from different neuronal types in the cochlear ganglion[73]. A prominent example of a rigid 2D penetrating architecture is the Utah array, which consists of a 10×10 grid of electrodes (100 channels) with 400 μm spacing, 50 μm exposed tips, and a total coverage area of 4.2 mm × 4.2 mm. The Utah array enables simultaneous recording from small neuronal populations with a signal-to-noise ratio of approximately 6:1, capturing an average of 3.4 neurons per electrode[74]. While these systems established the technological foundation for 2D deep-brain electrode arrays, their long-term implantation performance remains fundamentally constrained by the physical properties of rigid material platforms.

To alleviate chronic immune responses and signal degradation induced by rigid electrode structures, research has progressively shifted toward flexible 2D deep-brain electrode systems, with design priorities transitioning from structural strength-dominated approaches to strategies centered on mechanical matching with neural tissue. Common substrate materials include polyimide, Parylene C, PDMS, and hydrogels, whose Young's moduli more closely approximate that of brain tissue, thereby substantially improving mechanical compatibility. One representative example is the e-dura electrode, which employs a 120-μm-thick silicone substrate integrated with microcracked gold interconnects and 300-μm platinum-silicone electrodes. The device exhibits an impedance of approximately 5.2 kΩ and can withstand millions of stretch cycles at 20% strain, while incorporating microfluidic drug-delivery channels to support functional recovery following spinal cord injury[75]. Another example is the Neurotassel probe, which consists of individual flexible fibers with diameters below 10 μm that can be scaled to hundreds of channels and assembled into 2D arrays covering areas exceeding 1 cm^2 through capillary-force-driven self-assembly. Its exceptional mechanical flexibility arises from ultrathin polyimide encapsulation of nanoscale metal layers, resulting in extremely low bending stiffness and markedly improved mechanical matching with neural tissue[76]. The NeuroWeb probe represents an alternative ultrathin 2D flexible architecture, composed of stacked hexagonal boron nitride (h-BN) and graphene layers with a total thickness of approximately 40 nm. The device achieves an optical transparency of 97.2%, a unit signal amplitude of ~122 μV, and a coverage area of ~25 mm^2, enabling intimate conformal contact with curved cortical surfaces while supporting optogenetic experiments[77,78].

These 2D architectures reduce interfacial and mechanical constraints for large-area recording, but are inherently limited in probing volumetric neural activity, motivating three-dimensional designs.

3D Electrodes. Although conventional 2D electrodes have established a mature technological framework for planar cortical signal acquisition, they remain fundamentally surface-covering interfaces and are therefore limited in their ability to capture the volumetric structural and functional complexity of neural systems. In applications such as electrophysiological recording in the spinal cord[79] or the cochlea[80], neural activity is distributed across layered or spiral anatomical architectures. These intrinsic anatomical features directly motivate the development of 3D volumetric electrode systems capable of accessing neural activity throughout a tissue volume[81–91].

Early implementations of 3D architectures were realized by introducing vertical dimensions into conventional planar fabrication processes. Representative designs include 3D microelectrode arrays (3D MEAs) fabricated using two-photon polymerization (2PP), which enable direct printing of high-aspect-ratio probe structures on planar substrates. Following metallization and conductive polymer deposition, these electrodes can achieve impedances as low as 35.2 kΩ at 1 kHz, supporting high signal-to-noise ratio recordings in 3D neuronal cultures and multilayer tissue models[92]. However, such architectures are largely limited to in vitro systems or shallow tissue applications, with restricted spatial coverage in volumetric neural tissues.

Building on these approaches, foldable and self-deploying architectures have been introduced to improve in vivo adaptability. A representative example is a pop-up flexible array fabricated using planar processing techniques, which exploits built-in mechanical stress to transform into a 3D configuration after implantation. The structure comprises nine surface electrodes with a spacing of 500 μm and four penetrating shanks, each carrying six electrodes with a spacing of 200 μm. Electroplating with platinum black reduces the electrode impedance from approximately 1.3 MΩ to ~20 kΩ at 1 kHz. This design enables simultaneous recording of cortical surface activity and signals

from multiple intracortical layers within a single integrated system, thereby extending the high-resolution capabilities of 3D MEAs to in vivo applications[93].

For larger and more anatomically complex targets, the localized 3D architectures described above remain insufficient. To address this challenge, the i360 spinal cord electrode array employs an ultrathin (4 μm) Parylene-C membrane to achieve full 360° circumferential coverage of the spinal cord. The system integrates 32 interleaved channels that support simultaneous neural recording and electrical stimulation. In addition, topographic mapping enabled by this architecture allows functional discrimination between sensory and motor pathways[79].

As recording volumes expand substantially, long-term stability and tissue integration emerge as major bottlenecks for 3D neural interfaces. Injectable mesh electronics represent a representative strategy to address these challenges by achieving "structural conformality" with neural tissue through ultraflexible, highly porous architectures. For example, devices developed by Charles Lieber's group employ ultraflexible mesh structures with bending stiffness as low as ~0.1 nN·m and porosities approaching ~90%, enabling intimate integration with neural tissue. Delivered into the brain via syringe injection, the mesh electronics seamlessly interpenetrate the host environment. After 12 weeks of implantation, neuronal densities inside and outside the device recover to approximately 95% of baseline levels, with no significant increases in astrocytic or microglial responses, demonstrating excellent long-term biocompatibility and structural integration[94].

From a clinical translation perspective, endovascular approaches are increasingly emerging as an important direction for 3D neural interfaces. Compared with conventional craniotomy-based implantation, intravascular strategies substantially reduce surgical invasiveness and accelerate postoperative recovery[95,96]. For example, the Stentrode system is delivered via the jugular vein into the superior sagittal sinus, where recording electrodes are deployed intravascularly to enable minimally invasive, long-term ECoG recording[97,98]. Although the CereVasc eShunt system is primarily designed for cerebrospinal fluid diversion in communicating hydrocephalus, its clinical implementation demonstrates the engineering feasibility of delivering miniaturized devices through vascular pathways[99,100]. Collectively, these studies indicate that vascular routes may serve as a promising avenue for developing minimally invasive neural interfaces, while simultaneously imposing stringent requirements on device dimensions, bending stiffness, and structural flexibility. Building on endovascular strategies, Wang et al. developed an ultraflexible intravascular neural electrode, uFINE-1, which was successfully delivered to the occipital cortex of sheep. The device enabled recording of both spontaneous and visually evoked LFPs as well as single-neuron activity. Imaging and histological analyses revealed only minimal tissue damage and limited immune responses, underscoring the potential of intravascular microelectrodes as minimally invasive and stable neural interfaces[101].

Electrode dimensionality defines spatial sampling in neural recording, with 1D architectures enabling depth access and 2D architectures providing planar coverage. While these geometric choices establish the structural basis of neural interfaces, they are insufficient to ensure stable long-term performance. Under chronic implantation, recording stability is dominated by material properties, including electrical behavior, mechanical compliance, and interfacial biocompatibility. As BCIs move toward long-term and scalable operation, geometry-only optimization becomes inadequate, underscoring the need for material-centered frameworks and coordinated material-structure co-design.

As recording scale and system complexity increase, mechanical compatibility between neural electrodes and soft brain tissue becomes a critical factor governing long-term performance. Traditional rigid electrodes can induce chronic tissue response and micromotion-induced damage, which degrade signal stability over time. This has driven the transition toward flexible and compliant electrode structures that better conform to neural tissue and reduce mechanical mismatch. Such mechanically adaptive designs are essential for maintaining stable chronic recordings and enabling high-density, large-scale neural interfaces. Detailed system-level design strategies for achieving high-resolution neural recording will be further discussed in "*Design Strategies of Electrode Arrays for High-Resolution Neural Recording*".

Electrode materials for BCI

Conductive materials constitute the core component of brain-computer interface electrodes, serving as the physical and electrical interface between neural tissue and external electronic systems. Their primary role is to provide a stable electrical interface that enables coupling between neural activity in the biological environment and external recording or stimulation circuitry. The electrical conductivity and interfacial stability of these materials directly determine key electrode performance metrics, including impedance, noise level, and the safe operating range for electrical stimulation. Consequently, material selection critically influences signal fidelity as well as the long-term reliability of neural interface devices. Table 2 provides a comparative overview of representative electrode materials across these key performance metrics, highlighting their respective advantages and limitations. These performance dimensions are discussed in detail in the following subsections, organized by material class.

Metal electrodes. Metallic materials have long been regarded as the most reliable conductive systems for neural electrodes. Commonly used metals include gold (Au), platinum (Pt), iridium (Ir), platinum-iridium alloys (Pt-Ir), and tungsten (W), as well as metal-based oxides and nitrides such as iridium oxide (IrOx) and titanium nitride (TiN). The primary advantages of these materials lie in their high electronic conductivity, wide electrochemical stability windows, and favorable biocompatibility, which together provide long-term structural and electrochemical stability in complex physiological environments. In addition, metallic materials are highly compatible with conventional microelectronic fabrication processes, facilitating the realization of high-channel-count neural interface devices. However, the intrinsically high Young's modulus of metals (typically exceeding 100 GPa) leads to a pronounced mechanical mismatch with soft neural tissue (Young's modulus ~1 kPa)[102]. Moreover, the limited effective surface area of dense metallic electrodes leads to relatively high impedance, which constrains the acquisition of weak neural signals and exacerbates noise under chronic implantation conditions. To reduce impedance, surface roughening and functional coatings are widely employed to improve the performance of metallic electrodes by increasing the effective surface area without compromising the intrinsic stability of the metal[103]. Nanoporous platinum represents one of the earliest and most mature approaches, in which electrochemical deposition creates a 3D interconnected porous structure on the platinum surface, substantially increasing the electrochemically active area and improving signal-to-noise ratio. Similarly, sputtered iridium oxide films (SIROF) have proven highly effective as functional coatings. Optimized SIROF layers with thicknesses of approximately 660 nm exhibit impedances as low as ~4.8 kΩ at 1 kHz and a maximum reversible charge storage capacity of ~2.3 mC cm^{-2}. More importantly, SIROF-coated electrodes demonstrate high electrochemical durability, showing negligible changes in impedance and charge storage capacity after up to 2.76×10^8 cycles of high-intensity electrical stimulation, and maintaining stable performance over months of in vivo operation[104]. Beyond oxide coatings, alternative surface-structuring strategies have also been explored. For example, Ag-Au co-electrodeposition followed by selective etching has been used to generate 3D honeycomb-like porous structures on gold films with pore sizes on the order of 100–500 nm, effective electrochemically active surface area by several tens of times. Microelectrodes fabricated using this approach exhibit impedances of ~15 kΩ at 1 kHz and charge injection capacities of ~1 mC·cm^{-2}, while retaining structural robustness under mechanical agitation, making them suitable for high-resolution cortical microelectrode arrays[105]. Collectively, these surface roughening and pseudocapacitive coating strategies simultaneously achieve low interfacial

Table 2 | Electrode materials for BCIs

Materials Categories	Specific materials	Numbers of channels	Coverage area(mm)	Conductivity	Impendance	Young's modulus	Long-term stability (day)	Ref.
Metal-based materials	Zn-Mo	Single chemical unit	100 mm^2	0.2 Ω/mm	/	Zn:0.251 ± 0.092 MPa; Mo:0.509 ± 0.267 MPa	19	120
	Si NM, PLCL-PLGA	16 (passive)/ 32 (active)	200 × Initial area (diameter 70 mm)	/	~15 kΩ(at 1 kHz)	350 MPa(PLCL-PLGA)	17	118
Semiconductors	Si-NR; Au serpentine electrodes	2	100 mm^2	IOP sensor resistance: 2147.0 ± 203.3 Ω OST sensor resistance: 314.4 ± 13.14 Ω	/	Si-NR:GPa range PDMS substrate:MPa range	1	132
	C8-BTBT	1	15 × 15 mm^2	/	/	/	>30	251
	PEDOT:PSS	/	4 mm^2	/	6.3 kΩ(at 1 kHz)	0.4 MPa	28	128
	NBR + SEBS + OTS	54	3.3 transistors/mm^2	/	low impandence	Similar to human skin	one third	130
Hydrogel materials	β-peptide/carbon nanotubes (CNT)	/	/	0.1345 S m^{-1}	<200kΩ	~1500 Pa	/	240
	silver-nanowire/PVA hydrogel/melamine sponge (AgPHMS)	10	~3.14 mm^2 (single electrode)	/	6–8.5 kΩ	58.6 kPa	one second	248
Carbon-based materials	Graphene oxide (GO)	1 (Wet spinning)	Horizontal dimension:0.01–0.07 mm	1.50 × 10^5 S/m	/	340 ± 32 GPa	/	249
	Carbon nanotubes (CNT)	~0.06 tubes/mm	/	μ:64.2 cm^2/V·s	180 ± 50 kΩ per tube	/	/	250

impedance, high charge injection capacity, and excellent long-term electrochemical stability, thereby significantly improving the quality of weak neural signal recording (Fig. 2a)[106].

To address the mechanical mismatch between rigid metallic electrodes and soft brain tissue, an effective strategy is to minimize the metal thickness and introduce geometric patterning to achieve so-called "effective flexibility"[17]. For example, ultrathin platinum conductors (~200–300 nm) have been deposited onto polyimide substrates and patterned into serpentine interconnect geometries using standard photolithography and lift-off processes to form large-area electrode arrays. Mechanical characterization shows that these ultrathin serpentine metal structures maintain electrical continuity under bending radii below 1 mm and after more than 10^4 repeated bending cycles. Meanwhile, the electrode impedance remains stable in the range of ~20–40 kΩ at 1 kHz. This combined "ultrathin and serpentine" design markedly enhances the overall mechanical compliance of the device without sacrificing the intrinsic electrical conductivity of metals, making it particularly well suited for chronic cortical surface electrodes and peripheral nerve interfaces[107].

In microelectrode applications that require tissue penetration, the mechanical strength and chemical stability of electrode materials are critical. Traditionally, metals such as tungsten and platinum-iridium alloys remain the materials of choice. For example, tungsten needle electrodes with tip diameters below 1 μm can be fabricated using electrochemical etching combined with atomic layer deposition (ALD) insulation, enabling extremely small stimulation and recording volumes. Such tungsten microelectrodes exhibit stable in vivo performance over periods of weeks to months, with typical impedances of ~200–500 kΩ at 1 kHz, making them well-suited for single-unit and LFP recordings[108–110]. Another important recent trend is the use of highly porous TiN coatings to reduce electrode impedance in silicon-based neural probes. Under magnetron sputtering conditions, nanocolumnar TiN films with thicknesses of approximately 200–400 nm can be formed, yielding a rough and porous surface morphology that increases the effective surface area. Reportedly, TiN-coated electrodes with dimensions of ~20 × 20 $μm^2$ achieve impedances as low as ~50 kΩ at 1 kHz and maintain stable performance during long-term in vivo implantation[111]. These TiN-coated electrodes combine high electrical conductivity with favorable biocompatibility, making them a key material system for high-channel-count silicon neural probes. In summary, through nanoscale surface structuring and functional coatings, metallic electrode materials can achieve low impedance, high charge handling capability, and excellent long-term stability, thereby providing a robust foundation for high-performance brain-computer interface systems.

Carbon-based electrodes. Carbon-based materials, including graphene and carbon nanotubes (CNTs), are widely regarded as highly promising candidates for neural interface applications due to their unique combination of mechanical robustness and high electrical conductivity[112]. Graphene, for example, exhibits a Young's modulus of ~340 GPa, enabling the formation of ultrathin yet mechanically stable films that can conform closely to neural tissue. Carbon nanotubes, by contrast, offer high carrier mobility and intrinsically fibrous, porous architectures, which enhance electrode-tissue contact and improve electrical performance. Early applications of carbon-based materials in neural electrodes primarily focused on coating strategies, in which CNT or graphene layers were deposited onto conventional metallic electrodes. Such coatings significantly reduced interfacial impedance and increased charge storage capacity, thereby improving signal quality without fundamentally altering the underlying electrode architecture.

Building on these advances, CNT-based electrodes have demonstrated charge injection limits as high as ~2 $mC{\cdot}cm^{-2}$ in retinal implant applications—approximately an order of magnitude higher than those of conventional metallic electrodes. This enhanced charge injection capability enables safer electrical stimulation within a wider operational range, allowing more efficient and reliable neural activation. More recently, research efforts have increasingly shifted toward fully carbon-based electrode systems. For example, transparent graphene-ITO neural microelectrode arrays with minimum feature sizes down to ~20 μm have enabled simultaneous in vivo electrophysiological recording—including single-unit

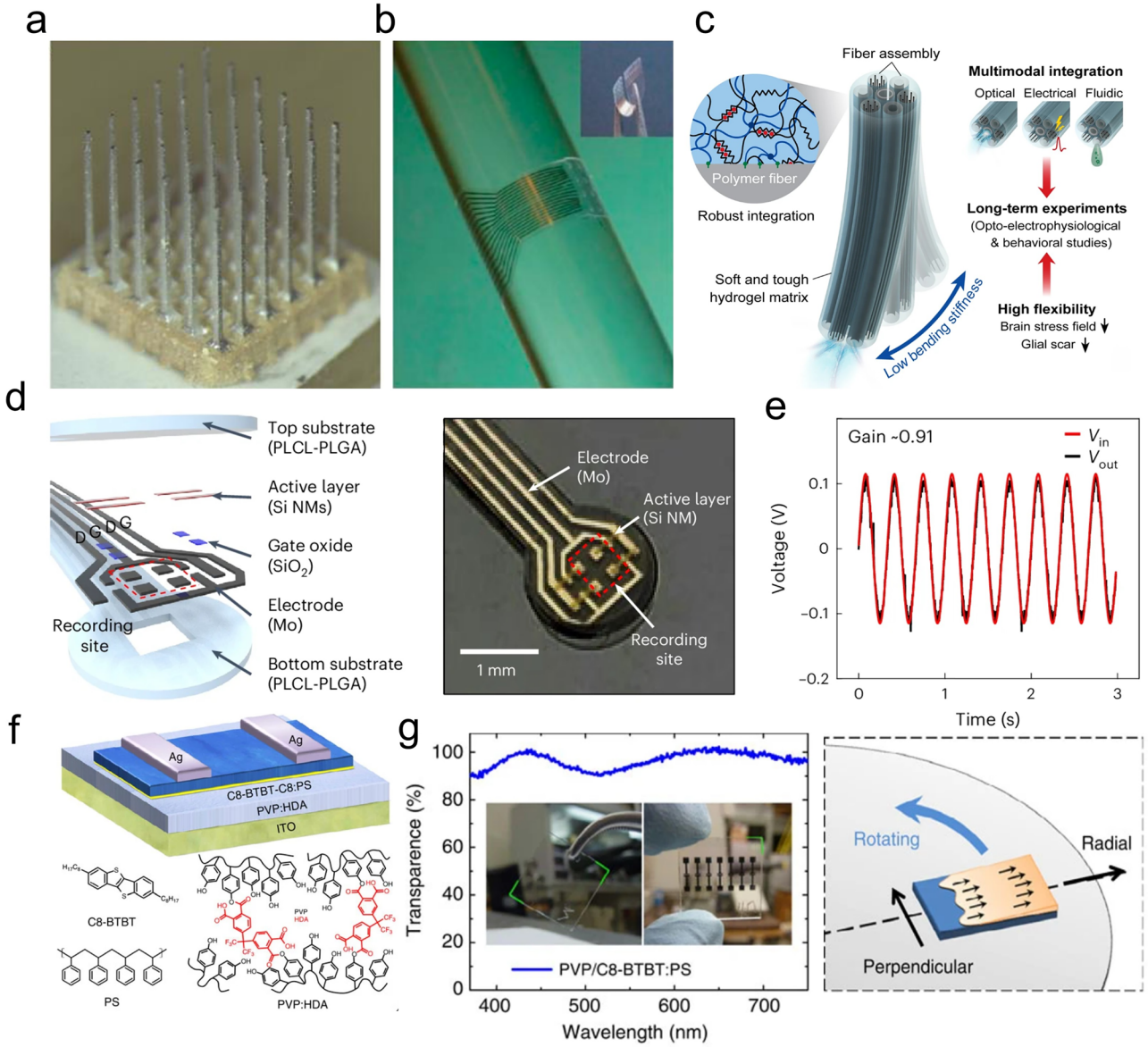

Fig. 2 | Electrode materials. a Microscopic characterization of a 6 × 6 aluminum-based microelectrode array (MEA)[106]. **b** Mechanical flexibility of a graphene-based CLEAR neural electrode, demonstrated by conformal wrapping around a 2.9-mm-radius glass rod. The ultrathin carbon film provides high conductivity, optical transparency, and mechanical compliance, illustrating key advantages of carbon-based neural interface materials[114]. **c** Design strategy for a hydrogel hybrid probe enabling chronic neural interfacing[117]. **d** Exploded view (left) and photograph (right) describe a 2 × 2 active electrode array mounted on a shared chassis. **e** The output response of such a unit under a 100 mV pp sinusoidal input is illustrated[118]. Copyright 2024, Springer Nature Ltd. **f** Schematic device configuration of an OTFT. **g** (Left) Schematic illustration of the off-centre spin coating (OCSC) process. (Right) Transmission spectrum of the PVP:HDA/C8-BTBT:PS film[251]. Copyright 2014, Springer Nature Ltd.

spike detection—and calcium imaging in freely behaving mice, combining optical transparency with robust electrical performance[113]. In parallel, chemical vapor deposition (CVD)-grown graphene thin-film microarrays have demonstrated stable impedance characteristics (~243 kΩ at 1 kHz) during long-term implantation periods of up to 70 days. Collectively, these studies illustrate a clear technological progression of carbon-based neural electrodes—from their initial use as functional surface coatings to fully carbon-based, multifunctional, transparent, large-area, and ultrathin electrode systems. Such developments position carbon materials as attractive platforms for chronic neural signal acquisition, particularly in applications that demand optical access, mechanical compliance, and long-term interfacial stability (Fig. 2b)[114].

Hydrogel electrodes. As an ideal material platform for soft neural interfaces, hydrogels excel in enabling mechanical matching with biological tissues (modulus range: 0.1–10 kPa) through tunable network structure and water content, while maintaining stable electrical performance[115]. Their 3D porous architecture (pore size: 1–100 μm) provides physical guidance for neuronal growth and supports tissue integration, while also enabling functional bioactive modifications[116]. In non-invasive applications, gradient modulus interfacial layers simultaneously match the epidermal stratum corneum (~1 GPa) and dermis (~0.1 MPa), achieving stress buffering from rigid integrated circuits to soft biological tissues. For invasive applications, dynamically adaptive hydrogel systems can accommodate local physiological changes, enabling progressive integration of electrodes with surrounding tissue (Fig. 2c)[117].

Semiconductor-based electrodes. The critical role of semiconductor materials in BCI electrodes arises from their tunable electrical properties and their ability to interface effectively with both biological and electronic

systems. Unlike conventional metallic electrodes, which rely exclusively on electronic conduction, semiconductors allow continuous modulation of conductivity and carrier density through band-structure engineering, doping concentration control, and defect-state management. This tunability provides a more compliant and adaptable electrical transition between neural bioelectrical signals and solid-state electronic circuits, enabling a "soft" electrical interface that is difficult to achieve with purely metallic conductors. Semiconductor materials employed in neural interface technologies can be broadly classified into two major categories: inorganic semiconductors, including single-crystalline silicon, silicon nanomembranes, and oxide semiconductors such as ZnO, IGZO, and In_2O_3; and organic semiconductors, represented by conjugated polymers and small-molecule systems such as P_3HT, and related materials. Together, these semiconductor platforms provide diverse pathways for engineering electrode interfaces that balance electrical performance, mechanical compliance, and functional integration in BCI systems.

Inorganic semiconductors remain the most mature platform for active neural interfaces. Single-crystalline silicon and silicon nanomembranes benefit from highly ordered lattices and mature doping control, enabling high carrier mobility, excellent device uniformity, and seamless compatibility with CMOS fabrication. These properties underpin their widespread use in high-performance neural recording and stimulation systems. However, even in ultrathin formats, silicon remains mechanically stiff and brittle, leading to significant mechanical mismatch with soft neural tissue and increased vulnerability to fracture under chronic micromotion. Moreover, silicon-based devices rely critically on encapsulation layers to block biofluids, and failure of these barriers can cause biofluid ingress, corrosion, and signal drift. Finally, current wireless implementations typically depend on non-biodegradable inorganic chips, limiting the realization of fully implantable and retrievable-free systems.

To overcome the intrinsic mechanical and biointerface limitations of silicon-based neural interfaces, significant advances have been achieved through improved material processing and structural design. By transforming silicon into ultrathin nanomembranes and integrating them with flexible polymer substrates, high electrical performance can be preserved while substantially improving mechanical compliance, enabling reliable chronic neural recording and stimulation. In parallel, chemically stable encapsulation layers—most notably thermally grown SiO_2—effectively suppress biofluid ingress and performance degradation, supporting long-term device stability. Figure 2d, e illustrate representative flexible neural interface systems based on inorganic silicon electronics. As shown in Fig. 2d, flexible silicon-based platforms integrate ultrathin semiconductor layers with soft substrates to realize mechanically compliant and multifunctional neural interfaces. These systems demonstrate that inorganic semiconductors can be engineered into flexible formats while maintaining high performance, supporting chronic implantation and stable operation[118]. In recent years, monocrystalline silicon platforms have further evolved through advances in materials processing and structural design. Submicron-thick silicon films have enabled flexible and stretchable devices[119] while biodegradable variants have opened pathways toward transient implantable systems[120,121]. Device formats have diversified to include non-invasive configurations such as direct scalp-mounted EEG interfaces121 and long-term packaging strategies now support operational lifetimes exceeding several years under accelerated physiological aging conditions[122]. Beyond planar formats, three-dimensional silicon architectures have enabled in vivo neural recording[123], and multifunctional nanofilm systems have incorporated additional sensing modalities such as pressure and temperature[124]. Collectively, these developments highlight the growing versatility of silicon-based platforms in neural interface technologies.

Beyond silicon, other inorganic semiconductors offer complementary advantages. III–V compounds such as GaAs and InP exhibit high electrical performance, supporting low-noise and high-speed signal processing[125,126]. Metal oxides such as ZnO further expand functionality by combining wide bandgaps with optical transparency. As illustrated in Fig. 2e, ZnO thin-film platforms demonstrate multimodal operation with high-fidelity electrophysiological recording (32.2 dB SNR) while maintaining optical accessibility, enabling simultaneous electrical and optical neural interrogation[127].

The development of organic semiconductors for neural interfaces has progressed from high-mobility small molecules to mechanically robust polymeric and composite systems. Early small-molecule semiconductors such as C8-BTBT and TIPS-pentacene enabled highly ordered π-π stacking and relatively high carrier mobility when combined with alignment strategies including off-center spin coating or vapor deposition. As illustrated in Fig. 2f, g, ultra-flexible C8-BTBT OTFTs achieved mobilities exceeding ~18 $cm^2 V^{-1} s^{-1}$ on flexible substrates, demonstrating that organic semiconductors can reach performance levels relevant for active neural electronics[128–130]. Building on these advances, polymeric semiconductors introduced in 2010s, including DPP-based polymers, P3HT, and thiophene derivatives, provided superior film-forming ability, mechanical flexibility, and solution processability for large-area and stretchable interfaces.

More recently, organic materials have evolved beyond simple conductive coatings toward multifunctional platforms for neural interfaces. Functional organic systems, including transparent nanomesh electrodes for concurrent optical stimulation and electrical recording[131], self-healing composites enhance device durability under repeated deformation[132] and biodegradable organic materials support transient implants with reduced long-term burden[133]. Meanwhile, organic semiconductor-elastic dielectric devices have achieved low-voltage operation and integrated sensing-pulse functions[134]. Building on these advances, organic materials are increasingly being developed to combine electrical performance, mechanical compliance, and biocompatibility within a single platform. Improvements in charge transport properties continue to narrow the performance gap with inorganic semiconductors, while the inherent softness and tunability of organic systems support stable long-term interfacing with biological tissues.

Organic mixed ionic-electronic conductors. Organic mixed ionic-electronic conductors (OMIECs), particularly conducting polymers such as PEDOT:PSS, represent a unique class of electrode materials that combine electrical conductivity with intrinsic mechanical softness and biocompatibility. Compared with metallic and inorganic semiconductor materials, OMIECs offer improved mechanical compliance and conformability, enabling stable interfacing with soft biological tissues.

Early materials such as PEDOT, PEDOT:PSS, and polypyrrole established the foundation for organic neural electrodes by significantly reducing electrode impedance and enabling flexible device formats[135–138]. Their integration into composite materials has further improved mechanical robustness and processability, supporting the development of wearable and implantable bioelectronic systems. Representative examples include transparent PEDOT:PSS-based interfaces with low impedance (~45 kΩ at 1 kHz)[139] and fully polymeric electrode arrays capable of maintaining stable neural recording under mechanical deformation[140]. Recent advances in molecular and supramolecular engineering have further expanded the material capabilities of OMIECs. For example, topological polyrotaxane-modified PEDOT:PSS networks enable the development of stretchable and photopatternable conductive films with high electrical performance, providing new opportunities for high-density and conformable biointerfaces[141]. These material innovations have been widely adopted in neural interface platforms. PEDOT:PSS-based systems have demonstrated stable electrical performance and long-term reliability in chronic cortical recording applications[142], as well as improved signal quality in soft and stretchable intraoperative neural interfaces[143]. In addition, conformable OMIEC-based electrode platforms have enabled high-density neural recording from the cortical surface in both animal models and human neurosurgical settings[144,145].

Collectively, these studies highlight the evolution of OMIECs from early conductive materials toward mechanically compliant, high-performance, and biointegrated platforms. Such developments position OMIECs as an important material system for next-generation neural interfaces that require softness, stability, and scalable integration.

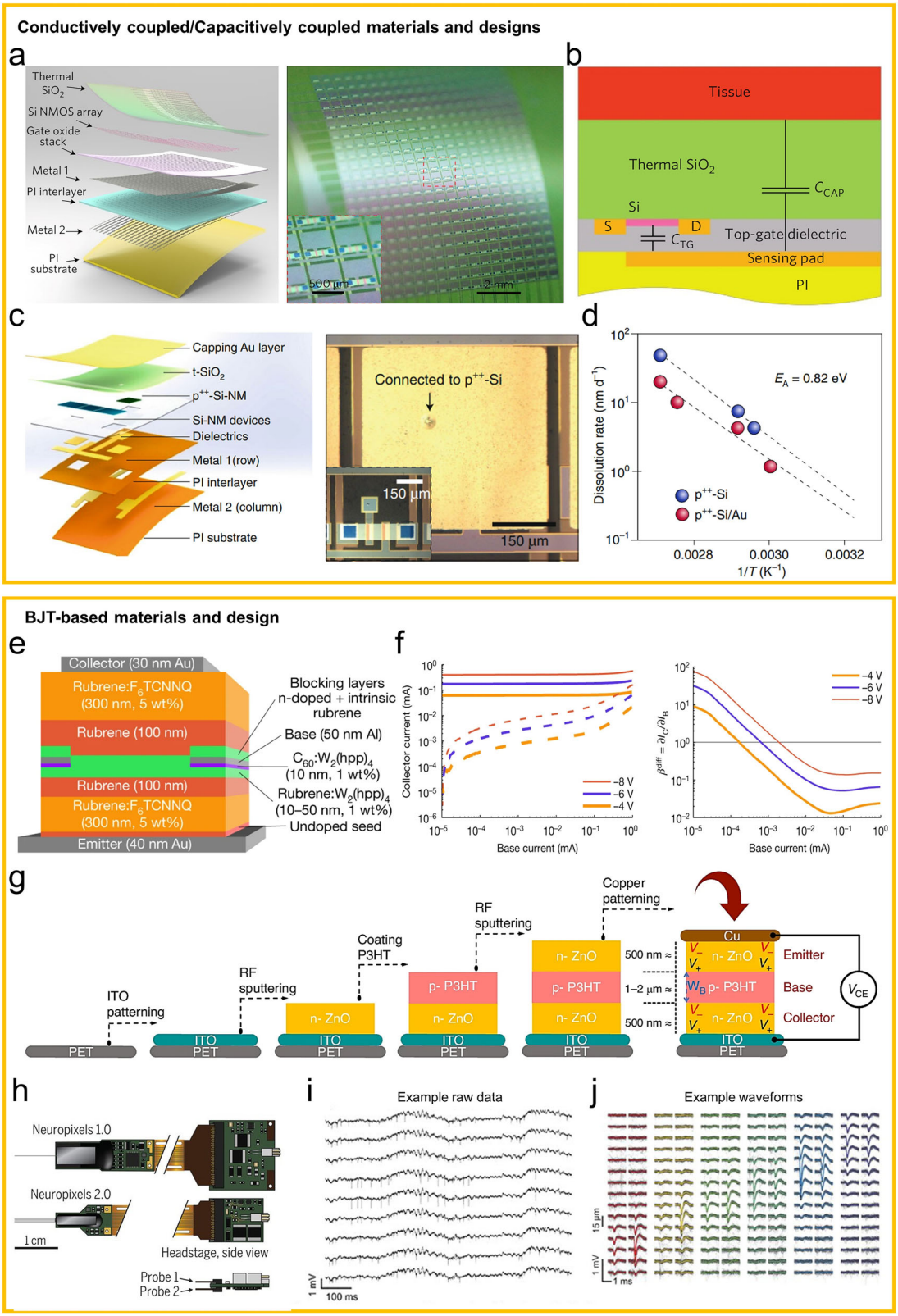

Microsystem architectures for neural signal recording

The signal transduction mechanisms described in this section are fundamentally governed by the intrinsic properties of electrode materials discussed in the previous section. Rather than reiterating material-specific descriptions, this section focuses on how these mechanisms-capacitive, Faradaic, and mixed ionic-electronic-manifest in signal characteristics and ultimately determine system-level performance in neural recording. Neural activity arises from ionic flux across neuronal membranes, which generates variations in extracellular electric fields[146]. These physiological processes form the basis of neural signaling, and the resulting activity can be represented and interrogated across multiple physical modalities, including electrical, optical, magnetic, mechanical, and chemical domains[147,148].

Fig. 3 | Active neural interfaces and signal transduction pathways. a Exploded-view schematic illustration (left) and a photograph (right) of a completed capacitively-coupled flexible sensing system. Inset on the right shows a magnified view of a few nodes. **b** The mechanism for capacitively coupled sensing through a thermal SiO_2 layer to an underlying transistor[155]. Copyright 2017, Springer Nature Ltd. **c** Left: mechanism for conductively coupled sensing through a hermetic-via structure to a Si-NM transistor. Right: image of a unit cell before (inset) and after deposition of a capping layer of Au, encapsulated by Au/p^{++}-Si//t-SiO_2. **d** Output characteristics of a representative sensing node in response to an ac input of 2.8 mV at 10 Hz[159]. Copyright 2018, Springer Nature Ltd. **e** Vertical stack configuration of the OBJT. **f** (left)Transfer characteristics of the OBJT device with blocking layers deposited on top of the base electrode for different V_{CE}: solid lines give the absolute collector current I_C, dashed lines give added current $\Delta I_C = I_C - I_{C0}$[274]. Copyright 2022, Springer Nature Ltd. **g** Device fabrication: Schematic of the fabrication steps of the n-p-n structure[275]. Copyright 2024, Springer Nature Ltd. **h** Comparison of Neuropixels 1.0 and 2.0 probes, showing reduced shank dimensions, higher site density, and updated on-shank CMOS amplification and multiplexing electronics. **i** Raw extracellular traces from adjacent channels, illustrating simultaneous LFP and spike capture enabled by the low-noise integrated front-end. **j** Example spike waveforms recorded across multiple sites, demonstrating high signal-to-noise ratio and spatial resolution supported by the dense electrode layout and on-shank signal conditioning.

Among these modalities, electrical and electrochemical transduction remain the dominant and most practically deployed strategies in implantable neural interface microsystems, due to their high temporal resolution and high signal bandwidth[148]. Thus, the fundamental objective of a neural recording microsystem is to transform the weak signals collected at the electrode-tissue interface into interpretable electrical information suitable for downstream processing.

At the electrode–tissue interface, neural signals are transduced through distinct interfacial electrochemical mechanisms, including capacitive coupling, Faradaic charge transfer, and mixed ionic-electronic conduction. These mechanisms define how ionic signals in the biological environment are converted into electronic signals in the device. Once the neural signal has been transduced at the interface, the raw output of neural electrodes consists of a complex mixture of extracellular field potentials (LFPs, 0.1–300 Hz, μV to mV range), high-frequency action potentials (spikes, 300–5000 Hz, tens to hundreds of microvolts), and various thermal and biological noise sources[149]. At this stage, the resulting neural signals are extremely weak in amplitude, broadband in spectral content, and highly susceptible to noise, leading to poor intrinsic signal-to-noise ratios. Therefore, an integrated neural recording microsystem is required to route, condition, and enhance these signals through amplification, filtering, noise suppression, digitization, and multiplexed acquisition, transforming them into structured data streams suitable for decoding and wireless transmission[150].

Signal transduction mechanisms in microsystems

Capacitive-coupled microsystems. Capacitive coupling is a fundamental interfacial transduction mechanism at electrochemically inert and ion-impermeable interfaces, where signal transfer is governed by interfacial capacitance rather than charge-transfer reactions. Traditional metallic microelectrode arrays (e.g., Pt and TiN) remain widely used and continue to serve as the foundation of implantable neural recording technologies[151]. Flexible CNT-based electrode arrays have been successfully demonstrated in vivo for stable and high-fidelity neural recording[152], and graphene-based implantable electrodes used in high-density flexible micro-electrocorticography (μECoG) arrays for chronic cortical recordings and have enabled stable single-unit spike recording with reduced interfacial impedance and improved long-term biocompatibility[153]. A variety of other capacitive-coupled architectures have further validated the robustness of non-Faradaic signal acquisition across extended implantation periods. Examples include NeuroGrid, a surface μECoG platform capable of recording both LFPs and superficial single-unit activity with stable performance in rodents and intraoperative human settings[154], flexible multiplexed silicon-dielectric arrays employing ultrathin dielectric encapsulation[155], and the Neural Matrix platform, which integrates ~1000 thermal-SiO_2-coupled channels with projected multiyear lifetimes in vivo[156]. Together, these demonstrations demonstrate scalability across materials, geometries, and species.

In these systems, neural signals are transferred via displacement currents across the electrical double layer (EDL) at the electrode-electrolyte interface without real electron-ion exchange. As illustrated in Fig. 3a, a representative implementation of a capacitively coupled array of multiplexed flexible silicon transistors FET system is shown[156]. This system is constructed on a polyimide (PI) substrate that provides mechanical flexibility, electrical insulation, and long-term biocompatibility. The platform integrates 396 independent sensor units arranged in an 18×22 array spanning a $9.5 \times 11.5\,mm^2$ footprint, with each unit occupying a 500×500 μm pixel. A multilayer metal/PI stack (Metal 1, PI interlayer, Metal 2) forms the local and global interconnect layers, routing signals between the sensing nodes and the periphery while preserving mechanical compliance. Above the interconnect stack lies a silicon nanomembrane (Si NM) NMOS transistor array, in which each 50-nm-thick Si NM transistor leverages its high carrier mobility for local amplification and buffering, with its intrinsic gate-oxide stack defining the electronic input node. The entire active area is encapsulated by a thermally grown SiO_2 dielectric layer approximately 900 nm thick, which provides a stable, ion-impermeable, and electrochemically inert barrier to the surrounding tissue. As shown in the cross-sectional schematic (Fig. 3b), neural activity in the tissue induces variations in the extracellular potential that are coupled across the thermal SiO_2 layer through an interfacial capacitance C_{CAP}. Because SiO_2 is electrochemically inert and prevents ion penetration, charge transfer occurs purely via displacement, realizing a capacitive coupling mechanism without Faradaic electron-ion exchange. The resulting voltage modulation at the sensing pad is subsequently coupled through the top-gate dielectric (C_{TG}) to the gate of the underlying MOSFET system, where it modulates the channel current for further on-chip processing.

As a result, the electrode output of capacitive coupling consists of weak extracellular analog voltage waveforms determined by charging and discharging dynamics at the interface. However, the purely capacitive interface exhibits relatively high impedance, which attenuates signal amplitude and degrades the signal-to-noise ratio. Consequently, capacitive electrodes are less effective for long-range signal transmission and applications requiring large charge injection, and are therefore predominantly deployed in stable, safe, and high-frequency neural recording modalities such as ECoG grids and microelectrode arrays for extracellular spike detection, where low electrochemical reactivity and high temporal resolution are essential[157].

Faradaic coupled microsystems. Faradaic coupling represents a fundamental interfacial electrochemical mechanism for neural signal transduction, in which ionic currents in the extracellular space are converted into electronic currents through reversible redox reactions at electroactive electrode surfaces such as IrOx, Pt black, or Ag/AgCl[158]. Local potential fluctuations modulate oxidation-reduction equilibria, enabling real electron-ion exchange across the electrode-electrolyte interface. This direct charge-transfer process results in low interfacial impedance and high charge-injection capability, making Faradaic interfaces particularly suitable for applications requiring strong coupling to neural tissue. As a result, Faradaic transduction is widely employed in neural stimulation modalities, including deep-brain stimulation, vagus nerve stimulation, and retinal prostheses, where efficient charge delivery is essential. However, because Faradaic processes rely on real electrochemical reactions, they also introduce inherent trade-offs in long-term stability and biocompatibility. Repeated charge transfer may lead to electrode degradation, interfacial corrosion, or the generation of undesired electrochemical byproducts, which can affect both device performance and tissue response over extended implantation periods.

In practical neural interfaces, Faradaic and capacitive contributions may coexist, with their relative contributions determined by material properties, surface structure, and operating conditions. This further highlight that interfacial signal transduction mechanisms are better understood as a continuum rather than strictly discrete categories. A practical implementation of a Faradaic coupled 2D electrode array is shown in Fig. 3c, d. The 64-channel flexible microsystem (8×8 configuration, 3.2×3.2 mm^2 active area) adopts a multilayer architecture consisting of a 1 μm thermal SiO_2 barrier, a 60 nm heavily doped p^{++}-Si nanomembrane, and an array of underlying NMOS transistors (channel length 16 μm, width 80 μm). Gold electrodes contact selectively exposed regions of the p^{++}-Si layer, forming a nearly 100% fill factor that maximizes the effective sensing area and enhances coupling efficiency. Neural potentials are transduced at the Au interface via weak and largely reversible interfacial charge-transfer processes, after which the resulting electronic currents propagate through the p^{++}-Si conduction layer into the transistor gate. At Faradaic interfaces, reversible redox reactions mediate direct charge transfer between ionic species in the electrolyte and electronic carriers in the electrode, thereby reducing impedance and improving coupling efficiency. This direct, solid-state faradaic pathway bypasses capacitive field-effect modulation and enables high-fidelity acquisition of low-frequency or large-amplitude neural signals. The multilayer stack is hermetically encapsulated to prevent biofluid penetration while maintaining mechanical flexibility. Accelerated aging tests performed in PBS at 96 °C (Fig. 3d) demonstrate excellent long-term stability, with a hydrolysis activation energy of 0.82 eV, confirming the robustness of the SiO_2/p^{++}-Si encapsulation and its suitability for chronic implantation[159].

Faradaic coupling enables low-impedance, high-fidelity transduction with exceptionally large charge-injection capability, making it indispensable for neural stimulation and for recording high-amplitude, deep-brain single-unit activity. However, because Faradaic transduction depends on real redox reactions, it also introduces challenges in long-term stability and biocompatibility. Repeated charge transfer may lead to material degradation, interfacial corrosion, or undesired electrochemical byproducts, thereby limiting long-term performance under chronic implantation. Taken capacitive or Faradaic interfaces together, mixed ionic-electronic materials allow ions to penetrate into the bulk of the semiconductor, enabling volumetric charge storage rather than surface-limited electrochemical coupling. This bulk ion-electron interaction produces exceptionally high capacitance and relatively low impedance, while simultaneously modulating the electronic conductivity of the channel to provide intrinsic amplification. Because these materials are soft, conformable, and operate through reversible doping processes rather than strong redox reactions, mixed-conduction interfaces offer enhanced mechanical compliance, long-term stability, and scalability for high-density neural recording microsystems[160]. The defining feature of mixed ionic-electronic interfaces is that the same ion-driven volumetric coupling that lowers impedance also produces channel modulation, effectively embedding a local amplification mechanism within the sensing material itself. This paper will discuss their amplification principles and implementations in detail in the following section.

Mixed ionic-electronic conduction. Mixed ionic-electronic conduction represents a distinct interfacial transduction mechanism in which ionic and electronic charge transport are coupled within the bulk of the material, rather than being confined to the electrode-electrolyte interface. In these systems, ions from the surrounding electrolyte penetrate into the active material and modulate its electronic carrier density through volumetric doping and dedoping processes.

This volumetric coupling enables substantially higher effective capacitance and lower interfacial impedance compared to purely capacitive interfaces, thereby improving signal transduction efficiency for weak neural signals. In addition, because signal modulation occurs throughout the material volume rather than at a two-dimensional interface, mixed ionic-electronic systems can achieve intrinsic amplification, making them particularly attractive for low-amplitude biosignal acquisition.

Neural interface platforms based on organic mixed ionic-electronic conductors (OMIECs), including PEDOT:PSS and organic electrochemical transistors (OECTs), exemplify this mechanism[161,162]. Representative examples include PEDOT:PSS-based neural interfaces such as NeuroGrid, which enable conformal cortical recording with high signal-to-noise ratios and simultaneous detection of local field potentials and action potentials[154]. In parallel, studies by Rivnay et al. have demonstrated that OMIECs enable volumetric capacitance and high transconductance in OECT devices, providing a direct physical basis for intrinsic signal amplification in bioelectronic systems.

However, the reliance on ion penetration and volumetric charge transport introduces trade-offs in response speed, stability, and long-term material integrity. As a result, mixed ionic-electronic conduction is particularly advantageous for high-sensitivity, low-frequency, and biointegrated neural interfaces, but may require careful optimization for high-bandwidth or long-duration applications. Importantly, mixed ionic-electronic conduction provides a conceptual bridge between capacitive and Faradaic processes, as it combines aspects of interfacial charge storage and volumetric charge transfer[163]. This further supports the view that neural signal transduction mechanisms form a continuum of electrochemical behaviors rather than strictly discrete categories.

System-level functional objectives

While interfacial electrochemical mechanisms define how neural signals are transduced at the electrode-tissue interface, their effective acquisition and utilization are ultimately governed by device-level architectures that control signal routing, amplification, and multiplexing within integrated microsystems. In particular, neural signals, once transduced at the interface, are conveyed through conductive pathways within the device, enabling their transmission from distributed recording sites to local processing units. Efficient interconnect design is therefore essential to minimize noise, signal loss, and wiring complexity in high-density neural interfaces.

At the system level, one of the most fundamental approaches to enhancing neural signal intensity is spatial or geometric integration, which can be regarded as a passive form of signal amplification. This mechanism arises from the physical area and volume over which an electrode collects neural activity. Larger electrodes integrate extracellular potentials generated by multiple neurons within their recording volume, producing substantially higher signal amplitudes, often in the millivolt range for local field potential (LFP) recordings, compared with microelectrodes that sample only one or a few neurons[164]. This population-level integration improves signal strength and signal-to-noise ratio (SNR) without requiring active circuitry, but inevitably reduces spatial specificity and obscures single-unit information, as neural contributions are averaged across both space and time[165]. As a result, such signals exhibit rich temporal, spectral, and network-level features, often requiring multidimensional analysis beyond spike-based representations.

Beyond passive mechanisms such as geometric integration, neural interfaces rely on active electronic amplification to boost weak extracellular potentials prior to digitization. Because neural signals typically fall within the tens of microvolts range, dedicated front-end circuitry is required to increase signal amplitude while minimizing additional noise. In parallel, multiplexing strategies are required to efficiently manage large numbers of recording channels, enabling scalable neural interfaces without excessive interconnect complexity.

Circuit-level signal amplification. Electronic amplification in neural interfaces is realized through cascaded MOSFET-based circuit blocks that condition microvolt-level extracellular potentials prior to digitization. At the core of nearly all analog front-end architectures is a low-noise amplifier (LNA), typically implemented using a PMOS-input differential pair with source degeneration and current-mirror biasing to achieve high input impedance, stable gain, and low input-referred noise. Because flicker noise is a dominant limitation in MOSFETs at low frequencies, many neural recording integrated circuits incorporate chopper-stabilized

stages, in which CMOS switches modulate neural signals to a higher frequency band for amplification and subsequently demodulate them, effectively shifting 1/*f* noise outside the signal passband[166]. Input buffering is commonly provided by source followers -common-drain MOSFET stages that offer unity gain while isolating the high-impedance electrode-tissue interface and improving drive capability. For capacitive or high-impedance electrodes, charge amplifiers based on MOSFET operational transconductance amplifiers (OTAs) with capacitive feedback are frequently employed to convert femto- to pico-coulomb charge variations into voltage signals with reduced sensitivity to electrode-impedance fluctuations and baseline drift. These amplification stages are complemented by on-chip active filters, typically realized using OTA-C or MOSFET-C topologies, which define the recording bandwidth, suppress DC offsets, and separate local-field-potential and action-potential activity[167,168]. Representative CMOS implementations highlight how these MOSFET-based principles translate into practical high-performance neural interfaces. A low-power biopotential amplifier fabricated in 28 nm CMOS integrates MOSFET-based active low-pass filtering and high-gain stages, achieving approximately 58 dB gain, a 7 kHz-3 dB bandwidth, and 11.1 μV input-referred noise in only 2500 μm^2 of silicon[169]. A complementary 180 nm CMOS analog front end combines a chopper-stabilized LNA with an automatic-gain-control amplifier using MOSFET current-mirror and source-degeneration techniques, achieving a dynamic range exceeding 80 dB within a 10 kHz bandwidth for closed-loop recording-stimulation systems[170]. Additionally, a CMOS readout circuit employing a differential MOSFET amplifier with capacitive-resistive feedback achieves high linearity and a noise-efficiency factor (NEF) of 2.53, demonstrating efficient action-potential and local-field-potential recording in legacy CMOS processes[171]. Collectively, these examples span three representative categories of CMOS neural front ends: a high-density, advanced-node amplifier; a closed-loop AGC architecture; and a classic NEF-optimized readout design, respectively.

As shown in Fig. 3h, a prominent example of integrated CMOS-based neural recording hardware is the Neuropixels 2.0 probe, which combines high-density microelectrode arrays with on-probe CMOS electronics for amplification, filtering, multiplexing, and data transmission. Fabricated using advanced CMOS microfabrication, this miniaturized silicon probe incorporates over 5000 electrode sites distributed across multiple shanks, enabling stable, long-term recordings from thousands of neurons in freely behaving small mammals. By embedding MOSFET-level front-end circuitry directly on the probe shank and base, Neuropixels 2.0 achieves low-noise amplification at the point of signal origin. The effectiveness of this on-shank MOSFET-based architecture is reflected in the high-fidelity raw extracellular recordings obtained by the probe, where microvolt-scale LFPs and high-frequency action potentials can be simultaneously captured across hundreds of sites with excellent signal-to-noise ratios (Fig. 3i). The clarity and stability of single-neuron spike waveforms across overlapping channels (Fig. 3j) further highlight the performance of the integrated CMOS front end.

Material-intrinsic signal amplification. Material-intrinsic amplification refers to signal gain that arises directly from the physical properties and charge-transport mechanisms of the sensing material itself, rather than from external circuit architectures or discrete amplifier stages. In such systems, the same material that interfaces with the biological environment actively participates in both signal transduction and gain generation. As a result, amplification is inseparable from sensing and can occur without relying solely on conventional low-noise amplifiers or purely electrostatic field-effect gating.

Organic electrochemical transistors (OECTs), and more broadly organic mixed ionic-electronic conductors (OMIECs), exemplify material-intrinsic amplification. In these materials, ions from the electrolyte penetrate into the bulk of the semiconductor and modulate its electronic carrier density through volumetric doping and dedoping processes. Unlike field-effect transistors, where charge modulation is confined to a thin interfacial channel, OECTs operate through 3D ion-electron coupling, giving rise to exceptionally large volumetric capacitance and transconductance. This volumetric transconductance enables substantial current modulation under low operating voltages, allowing mixed ionic-electronic materials to simultaneously transduce biological ionic signals into electronic currents and amplify them within the same active volume. As a result, OECTs are particularly effective for weak biosignal acquisition[172]. Recent advances include vertical OECT architectures enabling high-performance complementary circuits for bioelectronics[173], as well as ultrathin, soft, and even bioresorbable multichannel OECT arrays capable of high-resolution neural signal mapping on conformal tissue surfaces[174]. By contrast, vertical organic field-effect transistors (VOFETs), including organic permeable-base transistors (OPBTs), achieve high gain at low voltage through ultra-short channel lengths and vertical device architectures. For example, Shukla et al. demonstrated sub-50 nm channel lengths using perforated graphene source electrodes, enabling strong current modulation[175].

Beyond field-effect architectures, organic bipolar transistor concepts provide additional routes to intrinsic gain. One representative example is the vertically stacked organic bipolar junction transistor (V-BJT), in which highly crystalline rubrene thin films enable strong current amplification and GHz-level frequency response (Fig. 3e). These devices adopt a sandwich structure composed of a p-doped rubrene/gold emitter, aluminum finger electrodes with an n-doped rubrene base, and a p-doped rubrene/gold collector, with an overall thickness of ~1 μm to suppress parasitic capacitance. Amplification arises from minority-carrier diffusion: small variations in base current modulate the emitter-base junction, producing large collector current responses. Differential current gain can exceed 100 (shown in Fig. 3f) but decreases to ~10 as the base thickness increases from 20 to 50 nm, consistent with the measured diffusion length of ~50 nm. Notably, this amplification mechanism is purely electronic and device-intrinsic, distinct from ionic or mixed-conduction transistors.

Another promising strategy is the organic-inorganic hybrid piezoelectric bipolar junction transistor (PBJT), which integrates piezoelectric transduction directly with transistor amplification (as shown in Fig. 3g). The device consists of an ITO/PET substrate with a ZnO (n-type)-P3HT (p-type)-ZnO heterostructure capped by copper electrodes. Under external pressure, polarization charges in ZnO generate an internal electric field that forward-biases the emitter-base junction while maintaining a reverse-biased collector-base junction, enabling transistor-level current amplification. Injected carriers are swept by the collector field, producing amplified output currents that add to the displacement current. This architecture achieves high sensitivity (current mode ~139.8 kPa^{-1}; voltage mode ~88.7 kPa^{-1}), detects both static and dynamic inputs with response times below 110 ms, and operates in a self-powered manner.

Taken together, material- and device-intrinsic amplification strategies represent a spectrum of gain mechanisms that move beyond conventional circuit-level amplification by embedding signal gain within the sensing material or device itself. Mixed ionic-electronic systems such as OECTs and OMIECs achieve intrinsic amplification through volumetric ion-electron coupling, enabling exceptionally high transconductance and sensitivity under low-voltage operation, albeit with trade-offs in speed and long-term stability. Purely electronic architectures, including vertically stacked organic bipolar junction transistors, exploit minority-carrier diffusion to deliver high current gain and fast response, while hybrid approaches such as piezoelectric bipolar junction transistors integrate mechanical transduction with transistor amplification to enable self-powered and multimodal sensing. By contrast, vertical field-effect architectures rely on electrostatic short-channel control and therefore provide device-intrinsic rather than material-intrinsic gain. Collectively, these approaches underscore that no single intrinsic amplification mechanism simultaneously optimizes gain, bandwidth, mechanical compliance, and stability, highlighting the need to select or co-design amplification strategies according to application-specific requirements in neural and bioelectronic interfaces.

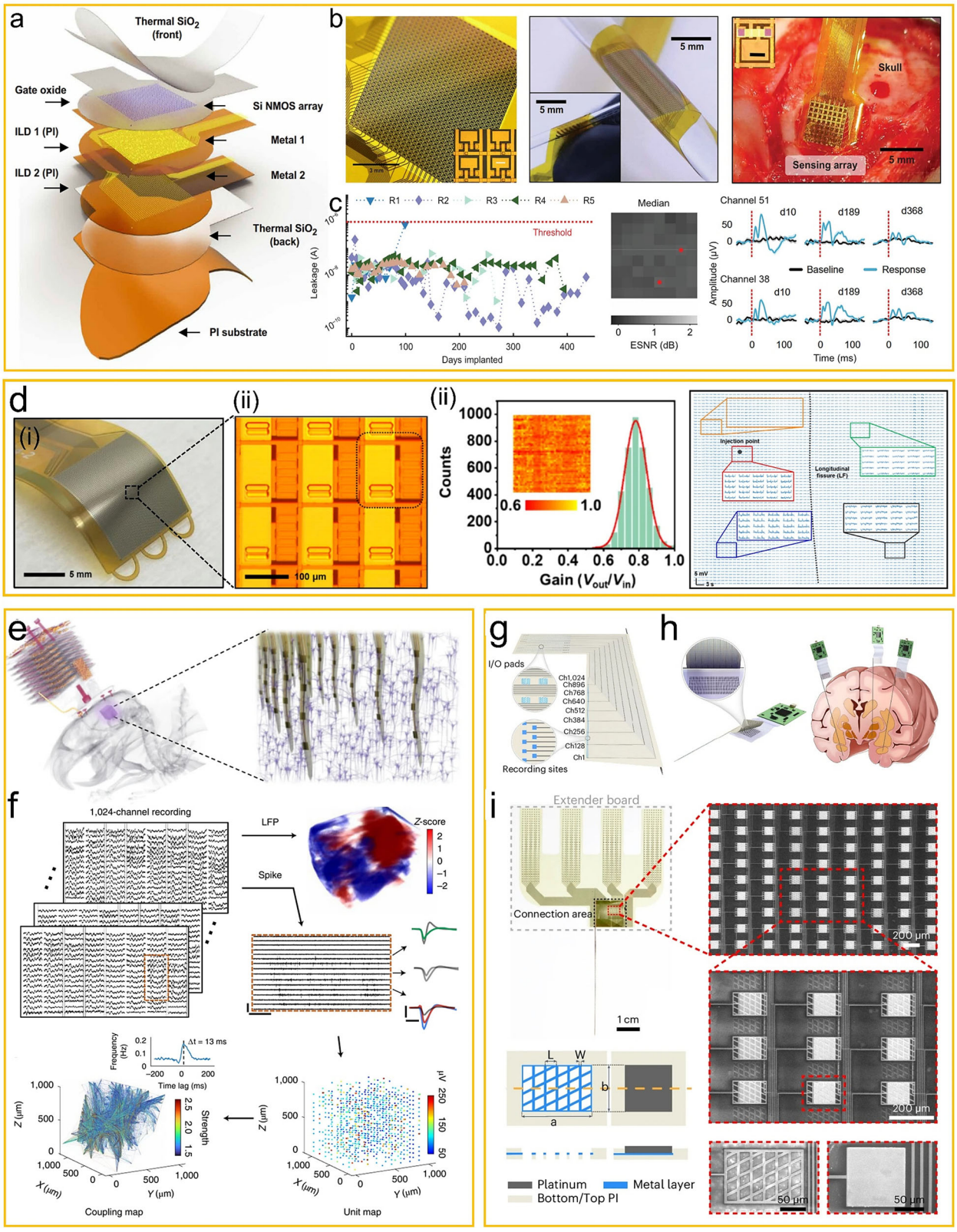

Design strategies of electrode arrays for high-resolution neural recording

BCIs technologies have historically focused on optimizing impedance matching, noise suppression, and interface stability at the level of individual electrodes. While these strategies have been effective in improving single-channel signal-to-noise ratios, they implicitly assume that neural information can be sufficiently captured at isolated spatial points. In reality, neural activity is inherently spatiotemporal and distributed across interconnected networks. Neuronal populations generate composite electric fields with cross-regional coupling on millisecond timescales, which propagate through brain tissue via volume conduction. As a result, individual electrodes primarily capture localized near-field signals and provide only a

Fig. 4 | The technical workflow of a high-density flexible neural electrode array. **a** Schematic of a flexible bioelectronic system (n-channel metal-oxide semiconductor (NMOS) transistor array, with t-SiO_2 (900 nm thick) as encapsulation. **b** Image of the active region of system (>1000 channels), in flat (left) and bent (middle) states. Scale bar, 100 μm.(right) Scalable system implanted onto the auditory cortex of a rat, with t-SiO_2 encapsulation. **c** (left) Leakage current at various intervals during chronic operation in rat models (R_1-R_5). (right)Click-evoked response at two nodes on different days, within 368 days after implantation[156]. Copyright 2020, Springer Nature Ltd. **d (i,ii)** Optical and magnified microscope images of the Neuro Cam array. The dimensions of each pixel unit and the corresponding gold sensing pad are 150 μm × 150 μm and 135 μm × 70 μm, respectively. **(iii)** Gain (Vout/Vin) characteristics of all 4096 channels in the array measured in PBS, with an input sinusoidal signal of 1 mV amplitude at 12 Hz. ECoG activity recorded from all 4096 channels during epileptic status, with insets showing zoomed-in schematic signals from different brain regions[182]. Copyright 2025, Elsevier. **e** Left: a micro-CT scan of an implanted NET array in a rat brain. **f** (up) Representative recordings from 1024 channels in an animal typical waveforms are depicted. Scale bars, 100 μV (vertical) and 1 ms (horizontal). Volumetric recording enables reconstruction of unit location (right) and mapping of pairwise correlation (left). The amplitude of units and the coupling strength are color coded[145]. Copyright 2023, Springer Nature Ltd. **g**, **h** Design schematic of the Neuroscroll probe featuring mesh-structured I/O pads. **i** Photograph and SEM images of a 50 mm long, 1024-channel Neuroscroll probe connected to a flexible extender board using the FCB method. Schematics show the top and side views of the mesh I/O pads and the corresponding pads on the extender board. The mesh consists of metal traces supported by a single PI layer[185]. Copyright 2024, Springer Nature Ltd.

partial view of underlying neural dynamics, failing to adequately reflect cross-regional coordination or hierarchical network organization. From this physical and informational perspective, the transition from single-point sensing to array-based neural interfaces is not merely advantageous but fundamentally necessary[54,147].

Once neural recording shifts from isolated electrodes to spatially distributed arrays, the design problem expands from single-channel optimization to system-level considerations. In chronic implants, electrode degradation (including impedance increases, glial encapsulation, and mechanical fatigue) is widespread[176,177]. When recordings rely on only a few sites, the failure of a single channel may compromise data continuity, whereas array-based architectures inherently provide redundancy and fault tolerance by enabling overlapping spatial coverage. Beyond reliability, the microvolt-level amplitude of neural signals renders large-scale recordings highly sensitive to thermal noise and electrochemical drift. As channel counts and spatial coverage increase, array-based systems inevitably encounter new scaling constraints related to signal integrity, interconnection complexity, power management, and long-term stability. Addressing these challenges requires coordinated optimization across materials, device architectures, and microsystem integration, which forms the central theme of the following sections[178,179].

Active 2D arrays

As electrode arrays increase in density, purely passive architectures encounter fundamental electrical limitations, including signal attenuation, inter-channel crosstalk, and unfavorable scaling of wiring complexity[180]. These constraints mark the first critical bottleneck in array-based neural interfaces and motivate the transition from material-driven flexibility toward electrically active array designs.

In 2D surface arrays, flexible μECoG technology first demonstrated the feasibility of array-based chronic recording. Khodagholy et al. introduced the NeuroGrid, which employed organic conductors and ultrathin flexible substrates to simultaneously resolve action potentials and field potentials on the rodent cortex[154]. Building on this foundation, Tsai et al. developed the Neural Matrix, which integrated capacitive coupling with dual-transistor units into a flexible μECoG platform, providing an important proof of concept for chronic, high-resolution surface recording[181]. The system incorporated 1008 channels, each connected to a circuit unit composed of two flexible silicon transistors specifically designed for chronic μECoG applications (Fig. 4a). Using a thermally grown ultrathin SiO_2 encapsulation layer, the device formed a capacitive coupling system with excellent flexibility, capable of bending around cylinders with radii of 2.5 mm and 1.25 mm, enabling long-term adhesion to complex cortical surfaces (Fig. 4b). In acute rat experiments, a 64-channel Neural Matrix implanted epidurally in the auditory cortex successfully resolved field potentials under 0.5-32 kHz tonal stimuli. In chronic recordings, leakage current remained below the safe threshold of 1 μA. Despite these advances, increasing array density further exacerbates the limitations of partially passive architectures. To address this challenge, Xie et al. proposed NeuroCam, a flexible high-density μECoG array based on an active-matrix architecture employing metal-oxide thin-film transistors (TFTs)[182].

In this design, each electrode node is equipped with an independent switching transistor, forming a 64 × 64 array with 4096 channels (Fig. 4d). The pixel unit has a size of approximately 150 μm × 150 μm, the gold electrode measures about 70 μm × 135 μm, and the overall device thickness is less than 30 μm, achieving ultrathin flexibility while providing an electrode density of 44 sites mm^{-2}. The system uses an active-matrix multiplexing architecture, enabling high-channel-count signal readout with only about 100 interconnect lines, effectively decoupling channel count from wiring complexity. Importantly, the architecture is compatible with mature display-industry fabrication processes, offering a scalable and potentially low-cost pathway toward dense surface arrays. In a rabbit epilepsy model, NeuroCam enabled spatiotemporal imaging of epileptiform discharge propagation and precise lesion localization with a spatial resolution of approximately 150 μm. However, while active-matrix architectures primarily address how neural signals are locally transduced, conditioned, and multiplexed at high channel densities, they do not fundamentally determine where those signals are sampled in space. Consequently, complementary design strategies have been pursued to expand the dimensionality of signal acquisition, either by extending recording coverage across large cortical surfaces or by enabling 3D access to distributed neural circuits.

Large-area surface arrays for extended cortical coverage

While active-matrix architectures alleviate interconnection bottlenecks associated with high channel density, expanding array coverage to the centimeter scale introduces a new set of constraints. As surface area increases, interface impedance, charge-transfer efficiency, and uniformity across large substrates become dominant factors limiting signal quality and spatial resolution.

Moses et al. addressed these challenges by developing PtNRGrids, which employ platinum nanorods to construct large-area 2D thin-film electrode arrays[183]. Unlike transistor-based approaches, PtNRGrids integrated thousands of channels on an 18 × 18 cm^2 glass substrate using thin-film fabrication. Arrays with 1024 and 2048 channels exhibited impedances of only 11 ± 2 kΩ and 8 ± 4 kΩ at 1 kHz, respectively, ensuring high spatiotemporal resolution across centimeter-scale cortex. In rodents, a 1024-channel PtNRGrid resolved sub-millimeter whisker responses, while in humans, the system captured fine temporal dynamics during grasp tasks and cortical propagation patterns of epileptic discharges with 1 mm spatial resolution. These results highlight the combined advantages of high channel density and large-area coverage, positioning such platforms as promising bridges between experimental neuroscience and clinical electrophysiology. Nevertheless, PtNRGrids remain limited to surface signals, lack extensive chronic validation, and require further advances in stimulation capability and integration density. In parallel, alternative strategies have pursued large-area surface recording through system-level integration rather than electrode-centric design. Flexible electronic and optoelectronic microsystems have enabled deterministic assembly of more than 32,000 wafer-level functional micro-units with interconnection areas approaching brain scale[162]. These platforms demonstrate good biocompatibility and long-term stability, with projected operational lifetimes spanning several decades and no observable leakage or performance degradation. Although their technical

pathways differ from conventional electrode arrays, such approaches represent complementary directions toward high-density, large-area surface recording.

3D Arrays for circuit-level access

Despite continued improvements in surface array density and coverage, 2D architectures remain fundamentally limited in their ability to access deep and layered neural circuits. To overcome this constraint, 3D implantable probes have emerged as a critical design direction, emphasizing ultraflexibility, minimal invasiveness, and volumetric access to neural networks. Zhao et al. developed ultraflexible penetrating nanoelectronic thread (NET) arrays that enable scalable three-dimensional neural recording across multiple brain regions, achieving long-term stable electrophysiological monitoring of thousands of neurons with densities approaching ~10^3 units/mm^3 in both head-fixed and freely moving animals[145].

Individual probes are approximately 1 μm thick, enabling stable recording with more than 1000 channels in mouse models. In vivo experiments showed that the 1024-channel NET array can simultaneously capture 8–12 Hz LFPs and >300 Hz high-frequency action potentials, reconstruct neuronal spatial locations and functional correlations at a density approaching 1000 units mm^{-1}, and maintain recording stability for several months (Fig. 4e, f). These NET-based architectures support chronic volumetric mapping of neural circuits over months, enabling the analysis of large-scale neuronal coupling and information flow with millisecond resolution. Other studies pursued minimally invasive implantation of ultraflexible microelectrode arrays into deep brain tissue, integrating them with optogenetic tools for simultaneous recording and modulation. For example, capillary-force-assembled elastic MEAs were combined with adeno-associated viral vectors carrying opsin genes, forming optoelectronic probes that enabled chronic recording and optical control in rodents[184]. Although employing different strategies, these studies shared the goal of overcoming surface array limitations and advancing chronic, large-scale circuit recording.

Extending this concept further, Fu et al. introduced the Neuroscroll probe, which employs a rolled architecture and flexible interconnects to create scalable, ultraflexible electrode arrays with adjustable lengths ranging from 10 to 90 mm (Fig. 4g)[185]. Using flexible cold bonding (FCB), Neuroscroll arrays achieved robust miniature connections to external amplification electronics through mesh I/O pads and extended cables, supporting both linear and clustered configurations. A 50 mm prototype incorporating 1024 channels demonstrated feasibility, while long-term studies reported stable recordings over two years in rodents and high-density single-neuron recordings across multiple cortical regions in macaques. By integrating scalability, mechanical robustness, and adaptable form factors, Neuroscroll outlines a promising pathway toward whole-brain electrophysiology, advanced neuroprosthetics, and closed-loop brain-computer interfaces.

In summary, the development of array-based neural interfaces has been guided by multiple scaling constraints that emerge as recording systems move beyond isolated electrodes. Electrically active 2D architectures provide an essential foundation by alleviating channel-density and interconnection bottlenecks. Building upon this foundation, distinct design strategies have been explored to address additional challenges associated with large-scale neural recording. Large-area surface arrays prioritize extended cortical coverage and low-impedance interfaces, while 3D probes pursue minimally invasive access to distributed and layered neural circuits. Together, these complementary approaches underscore that reliable, high-resolution neural recording cannot be achieved through a single design paradigm, but instead requires coordinated optimization across materials, device architectures, and scalable fabrication strategies. While these technological advances establish the structural foundation for next-generation BCIs, their ultimate impact depends on rigorous experimental validation in living systems. The following section, therefore, focuses on in vivo demonstrations that assess device performance, biocompatibility, and translational potential.

As neural interfaces scale toward 10^3–10^4 channels, they enable substantially enhanced spatial resolution, improved decoding performance, and more complete sampling of distributed neural population dynamics, thereby advancing high-dimensional brain state reconstruction and closed-loop neuromodulation. However, such scaling introduces fundamental system-level constraints in implantable environments. On-site signal conditioning, multiplexing, and CMOS-based digitization lead to a significant increase in power consumption, which is ultimately dissipated as heat within confined neural tissue. Given the low thermal conductivity of brain tissue (~0.5 $W\ m^{-1}\ K^{-1}$) and the absence of effective convective cooling, even modest increases in power density can produce non-negligible local temperature rises, imposing strict safety constraints for chronic implantation[186].

Recent large-scale neural interface systems have empirically highlighted this limitation. High-channel-count silicon-based probes such as Neuropixels have demonstrated that, despite rapid scaling beyond 1000 recording sites, in vivo operation remains constrained by strict power and thermal budgets to ensure stable long-term recordings[49]. More recent fully integrated CMOS neural interfaces and scalable cortical recording systems further confirm that power density, rather than physical integration density, becomes the dominant bottleneck when moving toward fully implantable high-channel-count architectures[78]. Across these systems, reported design constraints converge toward ultra-low-power operation in the sub- to few-μW per channel regime to maintain temperature increases below approximately 1 °C, widely regarded as the upper safety bound for neural tissue homeostasis. Importantly, these studies collectively indicate that thermal safety—not fabrication scalability—constitutes the primary limiting factor for fully implantable high-density neural recording systems[187–190].

From a physical standpoint, this limitation arises from the mismatch between rapid scaling of data throughput and the less favorable scaling of energy consumption in analog front-end amplification, analog-to-digital conversion, and wireless telemetry. As channel counts increase, cumulative static and dynamic power consumption scales nonlinearly due to shared clock distribution, interconnect capacitance, and continuous sampling overhead, making power efficiency the dominant constraint in system design.

To address these challenges, recent strategies have focused on ultra-low-power circuit architectures, including subthreshold analog front ends, event-driven or spike-based acquisition, and time-division multiplexing schemes that reduce simultaneously active channels. In parallel, emerging hierarchical and distributed architectures offload digitization and computation to external or intermediate nodes, thereby reducing on-implant energy dissipation while preserving high effective channel counts. More recently, system-level co-design approaches integrating electronics, packaging, and thermal modeling have been proposed to explicitly optimize the trade-off between spatial resolution, information throughput, and thermal safety.

Collectively, these studies establish that the scalability of neural interfaces is fundamentally governed by a coupled constraint space defined by power efficiency, thermal safety, and information bandwidth, rather than channel count alone[191–193].

Cross-level co-design in scalable neural interfaces

The performance of chronic neural recording systems does not arise from any single design layer, but instead emerges from coordinated co-design across materials, device architecture, packaging, and system-level integration. While individual advances in electrode materials or circuit design can improve specific metrics, scalable and stable neural interfaces require cross-level optimization to simultaneously address signal fidelity, mechanical compatibility, and deployment constraints.

A representative example of cross-level co-design is the integration of neural probes with CMOS electronics for large-channel-count recording, which fundamentally addresses the interconnect bottleneck in scalable neural interfaces. In conventional systems, each electrode requires an individual connection to external electronics, leading to rapidly increasing wiring complexity, limited channel scalability, and increased risks associated

with bulky packaging and implantation. By contrast, probe-CMOS integration enables on-site signal amplification, filtering, and multiplexing directly at the recording interface, allowing large numbers of recording sites to be accessed through a substantially reduced number of output connections. High-density systems such as Neuropixels exemplify this approach, demonstrating how coordinated design between probe geometry, interconnect architecture, and integrated circuitry enables scalable recording from hundreds to thousands of channels. More recent work by Jung et al. further extends this paradigm by introducing a fully integrated, wireless subdural brain-computer interface in which a 256 × 256 electrode array (65,536 electrodes) is monolithically combined with on-chip amplification, digitization, power management, and wireless data telemetry within a single CMOS platform[194]. Through local signal processing and multiplexed readout, the system supports simultaneous acquisition from up to 1024 channels while drastically reducing interconnect requirements.

Beyond device design, deployment strategies such as robotic implantation platforms play a critical role in enabling scalable neural interfaces. For example, robotic insertion systems developed for high-density brain-computer interfaces enable rapid and precise placement of large numbers of flexible electrode threads while actively avoiding surface vasculature. Such systems can insert multiple electrodes per minute with micron-level accuracy, significantly improving placement precision and reproducibility compared to manual implantation approaches. These automated implantation strategies reduce variability across experiments and enable the reliable deployment of high-density probe arrays at scale. Importantly, they also address a key limitation of flexible electrode systems, whose low bending stiffness makes manual insertion challenging[195]. As a result, system performance is not solely determined by probe or material properties, but also by the reliability, precision, and scalability of surgical and deployment processes.

Advances in micro- and nanofabrication further illustrate the importance of cross-level integration in scalable neural interfaces. For example, electron-beam lithography (EBL) has enabled the realization of ultra-high-density neural probes with nanoscale interconnects and electrode features. In representative studies, EBL has been used to define electrode wiring with widths down to ~100–120 nm and submicron pitch, allowing dozens to over a hundred recording sites to be integrated within a single narrow probe shank while maintaining compact interconnect architectures[196]. Similarly, nanofabrication approaches combining high-resolution lithography with ultraflexible device architectures have enabled nanoelectronic thread (NET) probes with subcellular-scale dimensions. For instance, NET-based electrodes exhibit cross-sectional areas below 10 μm² and can be implanted with interprobe spacing as small as ~60 μm without inducing chronic tissue damage, while maintaining high signal-to-noise recording performance[197]. In addition, ultraflexible nanoelectronic probes with submicrometer thickness have been shown to integrate seamlessly with neural tissue and minimize glial scarring, enabling stable long-term recording[198].

Together, these examples demonstrate that achieving functional scalability in neural interfaces requires coordinated design across fabrication, device architecture, and readout electronics to manage interconnect density, signal routing, and power consumption. More importantly, they highlight that chronic neural recording performance is fundamentally a system-level property that emerges from interactions across multiple design layers[199]. As a result, future progress in scalable brain-computer interfaces will depend on integrated cross-level co-design strategies rather than isolated advances in individual components.

Experimental demonstrations and translational studies

Experimental studies in animal models are essential for evaluating neural interface technologies under realistic biological conditions. Beyond assessing clinical readiness, such studies provide direct insight into long-term in vivo performance, where mechanical micromotion, tissue responses, and physiological variability jointly influence recording stability. As BCIs are evaluated in increasingly complex model systems, from rodents to large mammals, non-human primates (NHPs), and ultimately humans, the requirements for device robustness and signal consistency become more stringent. In this progression, the ability to maintain stable, high-quality neural recordings over extended periods emerges as a more informative benchmark than short-term signal acquisition alone. Comparative evidence from animal studies, therefore, helps identify material systems, structural designs, and interface strategies that are more resilient to chronic implantation. These investigations not only guide translational development but also expose recurring failure modes and performance limits that are difficult to capture in simplified or short-term experiments.

In this stepwise framework, each model serves a distinct purpose. Rodents enable proof-of-concept validation in the sensorimotor cortex. Large mammals (e.g., sheep) assess chronic implantation performance and biocompatibility under human-like cranial conditions. Non-human primates support high-density, multichannel recordings in specialized cortical areas for complex behavioral decoding. Human studies target disease-specific regions, motor, language-related (e.g., Broca's area), or sensorimotor networks, for closed-loop neuromodulation (Listed in Table 3). These stage-specific differences reflect a progressive escalation in anatomical scale, signal complexity, and engineering requirements.

Rodent models

Rodent models, particularly rats (Rattus norvegicus), are widely used as initial testbeds for validating neural interface technologies due to their low cost, ease of handling, and partial anatomical and physiological similarity to the human nervous system. At this stage, rodent studies primarily focus on establishing basic device feasibility, material biocompatibility, signal fidelity, and short- to medium-term stability under in vivo conditions. Representative demonstrations include the implantation of bioresorbable intracranial pressure (ICP) sensors via craniotomy, in which PLGA films and bioresorbable adhesives are used to ensure cavity closure, while clinical-standard ICP probes provide reference measurements to verify sensing accuracy (Fig. 5a). Such experiments illustrate the reliability and stability of degradable bioelectronic sensors for chronic physiological monitoring in small animal models. This experiment primarily demonstrates the stability and long-term reliability of degradable sensors for chronic intracranial pressure monitoring. Figure 5a-c further present synchronous comparisons between wireless and conventional tethered neural recording systems in rats, using a Y-shaped signal splitter to simultaneously capture the same neural signals[200]. EEG data under pharmacological stimulation (baclofen and pilocarpine) were compared to validate the fidelity of the wireless system during free movement. These experiments show that rodents are suitable for assessing the fundamental performance and biocompatibility of implanted bioelectronic devices and provide standardized references for designing experiments in more complex animal models.

Large mammal models

After establishing basic feasibility in rodents, validation commonly progresses to large mammals such as sheep (Ovis aries), where human-relevant anatomical dimensions, vascular anatomy, and surgical access routes impose more stringent constraints on implantation, long-term stability, and safety. Representative stimulation studies in sheep demonstrate the feasibility of endocisternal neural interfaces (ECI) and magnetoelectric bioimplantable devices (ME-BIT) for wireless neuromodulation (Fig. 5d, e)[201]. The system-level layout includes intracorporeal electrodes and defined stimulation targets, together with an external magnetic-field emitter and wireless power/command components (Fig. 5d)[201]. Figure 5e demonstrates synchronized brain and spinal cord stimulation and time-locked CMAP recordings, validating multi-target stimulation and immediate functionality. Beyond acute stimulation, long-term feasibility has also been evaluated in sheep using endovascular stentrode interfaces (Fig. 5f). The left panel shows maximum bandwidth over different implantation periods, indicating stable bandwidth over 190 days (0–2 weeks: 197.4 ± 42.0 Hz; >20 weeks: 196.4 ± 20.7 Hz)[202]. The middle panel shows ex vivo synchrotron imaging of the superior sagittal sinus (SSS) lumen area, confirming patency after long-term implantation. The right panel presents in vivo angiography

Table 3 | Animal models for chronic BCI device development

Animal Model	Application Scope	Advantages	Limitations	Typical Implantation Targets	Key Engineering Challenges	Ref.
Rodents (mouse/rat)	Proof-of-concept studies, biocompatibility testing, single-unit neural recording	Low cost, mature genetic tools, short experimental cycles	Simplified brain architecture, limited cortical complexity, low translational homology	Primary motor cortex (M1)	Thin cortical layers increase risk of overshooting target depth; mismatch between brain micromotion and rigid electrodes; chronic signal drift	252–254
				Hippocampal CA1	Requires long shank electrodes for deep targeting; chronic drift limits long-term single-unit stability	255–257
				Sensory cortex (S1)	Limited network complexity; stimulation spread reduces spatial resolution	258
Large animals (pig/sheep/dog)	Device-level validation (packaging, wireless power transfer, chronic implantation systems)	Brain size comparable to humans, suitable for engineering validation	Limited behavioral paradigms, high cost, lower standardization	Superior sagittal sinus (endovascular stent electrodes)	Complex vascular access route increases catheter resistance; thrombosis risk due to poor stent apposition; unknown long-term hemodynamic effects	259,260
				Motor cortex (M1)	Skull thickness causes signal attenuation; challenges in thermal management for implanted electronics	261,262
				Subdural space (ECoG arrays)	High dural tension leads to electrode folding; increased risk of subdural hematoma compared with rodents	263
Non-human primates (NHPs)	High-level motor decoding, cognitive processing, pre-speech/language studies	High anatomical similarity to humans, complex behavioral training capability	Ethical constraints, extremely high cost, long training periods	Premotor cortex (PMd)	Requires long-term recording of hundreds of neurons for complex motor decoding; strict weight constraints for implants	264,265
				Posterior parietal cortex (PPC)	High non-stationarity; decoders require frequent recalibration; micromotion during active behavior affects stability	266,267
				Broca homolog region	Sparse speech-related neurons; requires high-density probes and long training cycles (>6 months)	268
Humans (clinical studies)	Final clinical validation (efficacy, safety, performance)	Direct clinical relevance and translational value	Limited experimental flexibility, high inter-subject variability	Primary motor cortex	Long-term implantation stability required (years); gliosis-induced signal attenuation; infection risk via percutaneous interfaces	269
				Broca/Wernicke areas	Strong inter-individual variability; requires functional mapping during awake surgery; high-density coverage needed for fine-grained speech decoding	270,271
				Anterior cingulate cortex (ACC, psychiatric neuromodulation)	Deep targets; requires precise vascular avoidance; strict latency requirement for closed-loop control	272,273

measurements of SSS diameter, showing no significant reduction from implantation day to 12 weeks (median 2.2 mm on day 0, 2.5 mm at 12 weeks). Overall, large-mammal models such as sheep offer physiologically and anatomically relevant conditions for assessing chronic stability, procedural feasibility (including minimally invasive delivery), and tissue/vascular safety, providing a critical validation step before NHP and human studies.

Non-human primate (NHP) models

To assess complex cognitive functions, non-human primates serve as a critical bridge for validating large-scale, high-resolution neural recording technologies. In macaque experiments, the Neuroscroll probe was implanted to enable stable recordings across multiple cortical regions (Fig. 5g). The probe features a high-density distribution of recording channels, supporting simultaneous acquisition of neural signals from spatially distributed brain areas (Fig. 5h)[176]. Also, Fig. 5i presents a motor task used to study macaque sensorimotor activity, where the monkey tracks points along a rolling path by generating isotonic force. The figure identifies recording targets in the motor cortex and M1 gyrus, demonstrating the probe's utility for monitoring neural activity during motor tasks. In addition, the Neuropixels 1.0 probe enabled simultaneous recordings from multiple brain regions, facilitating the study of inter-regional interactions and large-scale coordination in the primate brain (Fig. 5j)[203]. Overall, NHP models enable validation of neural interface technologies at scales of channel count, spatial coverage, and behavioral complexity that are not accessible in smaller animals, providing a crucial translational benchmark for human applications.

Human clinical studies

At the final stage of validation, neural interface technologies are evaluated in human clinical studies, where functional efficacy, safety, and real-world usability are directly assessed.

From a systems perspective, neural feedback links signal acquisition, state interpretation, and intervention execution, enabling neural interfaces to evolve from passive recording platforms to active closed-loop systems. In neural monitoring and diagnosis, signals acquired via EEG, ECoG, or intracranial electrodes enable the detection of abnormal activity and support early prediction using data-driven methods. Task-based BCI paradigms further allow assessment of covert awareness beyond behavioral measures. Wearable and minimally invasive sensors extend these capabilities to continuous monitoring of sleep, emotion, and attention states.

These signals can be incorporated into feedback loops to enable adaptive intervention.

For example, a multimodal feedback BCI system (as shown in Fig. 5k) integrates motor intention detection with proprioceptive, tactile, and visual feedback to promote cortical plasticity in stroke rehabilitation[204]. The process includes: (1) motor imagery, where chronic stroke patients simulate

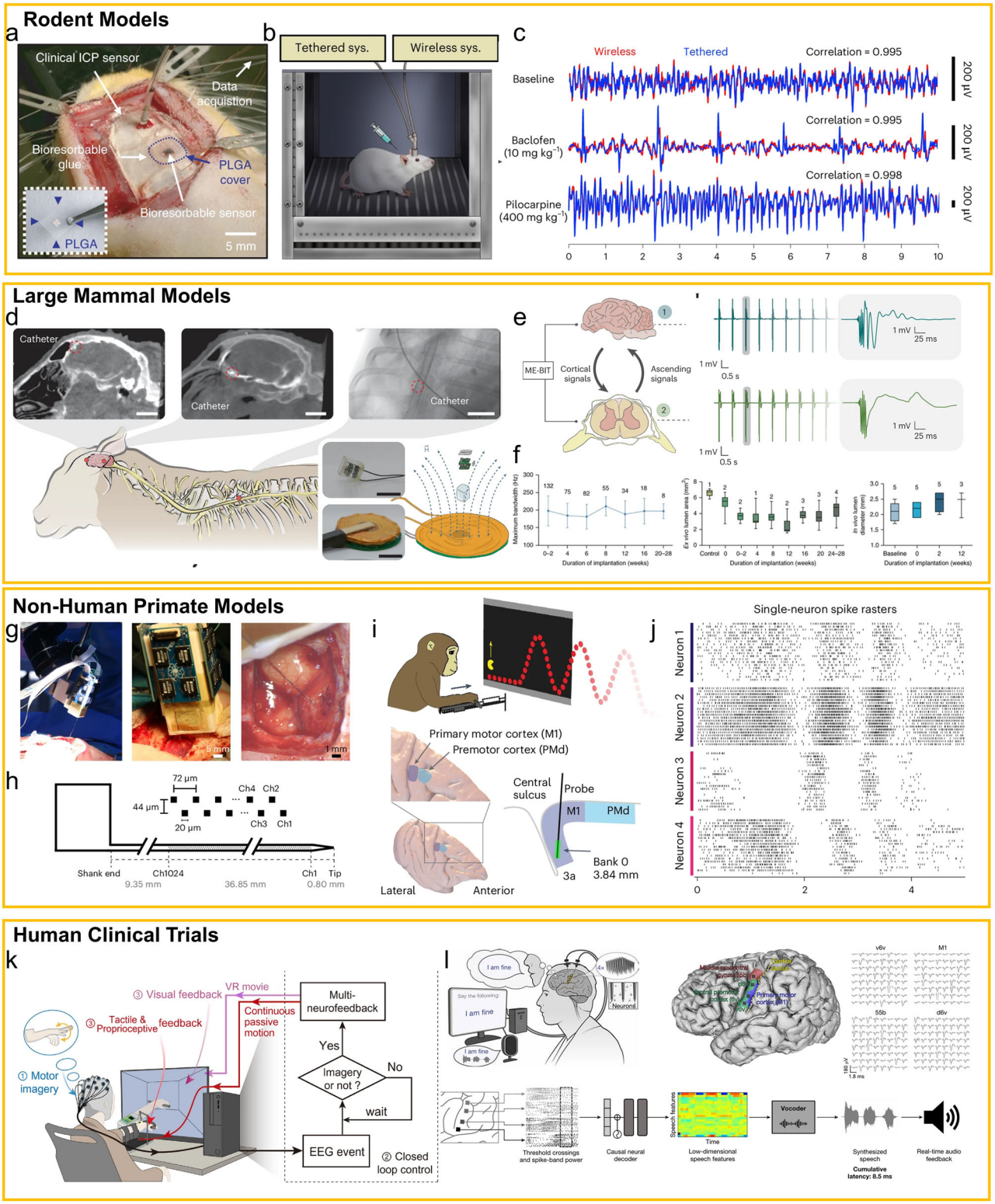

movements of a paralyzed limb (e.g., wrist flexion/extension) captured by EEG; (2) closed-loop control, where detection of motor imagery triggers multimodal feedback; (3) multimodal feedback, combining proprioceptive feedback via continuous passive motion (CPM) devices, tactile feedback via brush stimulation, and visual feedback via VR displays, forming a closed-loop neural regulation that promotes cortical plasticity. In therapeutic applications, neural feedback supports biomarker-driven neuromodulation. Responsive stimulation systems detect pathological activity and deliver targeted intervention, while adaptive strategies dynamically adjust stimulation parameters based on neural signals, improving efficacy and reducing side effects[33,34]. Feedback-guided modulation is also being explored for psychiatric disorders[35].

Neural feedback further enables functional rehabilitation through continuous sensing-feedback-relearning cycles. Figure 5l illustrates a brain-to-speech neuroprosthetic framework, using four microelectrode arrays (256 electrodes) implanted in the left precentral gyrus (including ventral/

Fig. 5 | The use of bioelectronic devices in animal models (rodents, large mammal models, non-human primate models and human clinical trials). a Photo of bioresorbable ICP sensor[276]. Copyright 2018, Springer Nature Ltd. **b**, **c** Schematic of A/B test setup[200]. Copyright 2023, Springer Nature Ltd. **d** (left) Motor-evoked potentials (MEPs) recorded from sheep hind leg via motor cortex stimulation; Middle: Slow cortical potentials (SCPs) recorded via deep brain (thalamus) stimulation; Right: Compound muscle action potentials (CMAPs) recorded from sheep back muscles via spinal cord stimulation. Lower: Left: Schematic of sheep, catheter electrode and neural stimulation positions; Right: Photos of magnetic field transmitter, magnetoelectric-powered implant and schematic of wireless system. **e** (left) Schematic showing the synchronized stimulation of brain and spinal cord. (right) Time-locked recordings of simultaneous brain and spinal cord stimulations[201]. Copyright 2024, Springer Nature Ltd. **f** Chronic viability of implanted stentrode. (left)Maximum observable bandwidth from recordings. (Middle) ex vivo SSS lumen areas. (Right) In vivo SSS internal lumen diameter via cerebral angiography[202]. Copyright 2016, Springer Nature Ltd. **g** Photos of probe implantation into monkey brain. **h** Schematics showing the distribution of the 1024 recording channels along the shank of probe 1[185]. Copyright 2024, Springer Nature Ltd. **i** Top, force tracking task. Bottom, recording targets in motor cortex (left) and schematic of recording target in sulcal M1, sagittal section (right). **j** Single-trial spike raster for four example neurons[203]. Copyright 2025, Springer Nature Ltd. **k** A Schematic of the experimental setup of Multi-FDBK-BCI therapy[181]. Copyright 2025, BioMed Central. **l** 1. Brain-to-voice neuroprosthesis; 2. Array locations on left brain hemisphere and typical neuronal action potentials of each microelectrode; 3. Closed-loop causal voice-synthesis pipeline[204]. Copyright 2025, Springer Nature Ltd.

dorsal 6v, M1, and 55b areas) to record speech-related neural activity[204]. Neural signals are decoded and synthesized into speech using a Transformer-based decoder and vocoder, with total latency as low as 8.5 ms, restoring speech function in ALS patients.

Similarly, BCIs can drive external effectors such as functional electrical stimulation or robotic systems to reconstruct motor pathways and enhance recovery[41–43]. With increasing capability, neural interfaces are extending toward health management and prevention. Long-term monitoring combined with feedback modulation can support sleep optimization, cognitive regulation, and early intervention in neurodegenerative diseases[39,40]. The overall research trajectory-from animal models to human application-follows a stepwise validation process, ensuring stability, reliability, and performance across increasing levels of complexity. Neural feedback is evolving from a simple signal modulation mechanism into a central paradigm that integrates neural monitoring, intervention, and long-term regulation. With continued advances in artificial intelligence, multimodal sensing, and wireless microsystems, neural interfaces are expected to achieve more precise, personalized, and autonomous closed-loop control, thereby accelerating their clinical adoption.

Frontier directions in BCI devices and microsystems

Recent advances in brain-machine interfaces have highlighted a broad set of limitations in conventional technologies. For example, chronic performance degradation is widely observed in implanted neural electrodes, including silicon microelectrode arrays, Utah arrays, and metallic microwires. Signal decline over time is primarily attributed to material degradation (such as electrode corrosion and insulation failure), mechanical mismatch that induces micromotion or dural tethering, and chronic neuroinflammatory responses involving glial encapsulation and neuronal depletion. These mechanisms jointly contribute to elevated impedance, diminished spike amplitudes, and reduced numbers of viable channels. Collectively, the foreign-body response to rigid implants, the inability to accommodate brain micromotion, and the constraints of purely electrical sensing represent key barriers to stable long-term recordings. As a result, recent research has increasingly focused on advanced materials, flexible architectures, and multimodal sensing approaches.

Biodegradable interface

To address the biological burden imposed by long-term implants and to avoid chronic foreign body reactions, researchers have explored transient bioresorbable neural interfaces. By allowing the device to harmlessly dissolve after completing its functional window, these systems eliminate the need for surgical retrieval and minimize chronic inflammation, while enabling short-term high-fidelity monitoring during acute or perioperative periods.

One prominent approach to bioresorbable electronics is "transient electronics", which was first introduced by Rogers and colleagues[205]. A representative implementation of this concept is illustrated in Fig. 6a.

In this design, a fully bioresorbable cortical electrode array is constructed by laminating a highly doped single-crystalline silicon (Si) nanomembrane (~300 nm thick) onto a 30 μm PLGA substrate, with an embedded 100 nm SiO_2 layer serving as insulation. The same Si nanomembrane functions simultaneously as the transistor channel and the electrode interface. A key innovation of this architecture lies in its fully predictable hydrolysis pathway: Si gradually dissolves into orthosilicic acid at ~11 nm day^{-1}, SiO_2 hydrolyzes at ~8.2 nm day^{-1}, and PLGA degrades over ~4–5 weeks, collectively defining an operational window of several days to several weeks. The ultrathin geometry further imparts mechanical compliance; serpentine interconnects enable bending down to a 1 mm radius while maintaining a principal strain below 0.03%, allowing stable conformal contact with the cortical surface. In awake-rat studies, the system delivered high-quality acute-to-sub-chronic ECoG and EEG recordings for up to 33 days, with performance comparable to clinical electrodes and minimal tissue response. Nevertheless, the limitations of this strategy are equally evident. As the Si nanolayer dissolves, changes in local doping concentration and electrical continuity become unavoidable, making it difficult for high-density active-matrix devices (>500 channels) to maintain synchronized end-of-life behavior[206]. These constraints highlight an inherent trade-off in inorganic transient electronics between precise electronic performance and controllable, uniform bioresorption, motivating the exploration of alternative material platforms.

In the domain of organic semiconductors, the transient OECT array shown in Fig. 6b represents a contrasting materials strategy. The device features an ultraflexible, fully organic architecture in which both the substrate and encapsulation layers are biodegradable polymers, while the transistor channels are formed from mixed-conductor PEDOT-based thin films. The resulting array—substantially thinner than 100 μm—integrates 100 lithographically patterned OECT units with ~20 μm spatial resolution, 1.42 ms temporal resolution, and an SNR of ~37 dB, enabling stable operation over a short functional window prior to complete hydrolysis. The inherently low operating voltage and high transconductance of OECTs make them particularly appealing for perioperative and other short-term monitoring scenarios. However, the organic channel materials are intrinsically sensitive to moisture, leading to an exponential decline in transconductance once degradation initiates. As device size or channel count increases, mismatches between the kinetics of material dissolution and the required functional lifetime become increasingly pronounced. These limitations currently prevent OECT-based transient systems from achieving reliable medium- or long-term implantation, underscoring the need for more stable semiconducting materials and device architectures for future bioresorbable neural interfaces[164].

Beyond Si[207] and OECT-based platforms, a broad spectrum of bioresorbable neural interface technologies has emerged to enable devices that exist only when needed and disappear on demand. Recent advances include transient CMOS systems constructed from ultrathin Si nanomembranes combined with soluble Mg or Zn interconnects to achieve programmable lifetimes[183]; injectable mesh electrodes that provide mechanically compliant, immunologically inert long-term interfaces[94]; in vivo-assembled, bioresorbable conductive hydrogel electrodes[208]; and miniaturized ultrasound-readable sensors that can be injected and subsequently degrade over weeks to months[209]. Additional strategies involve stress-engineered PLGA/Au microtube electrodes[210], fully degradable metal-polymer microelectrodes

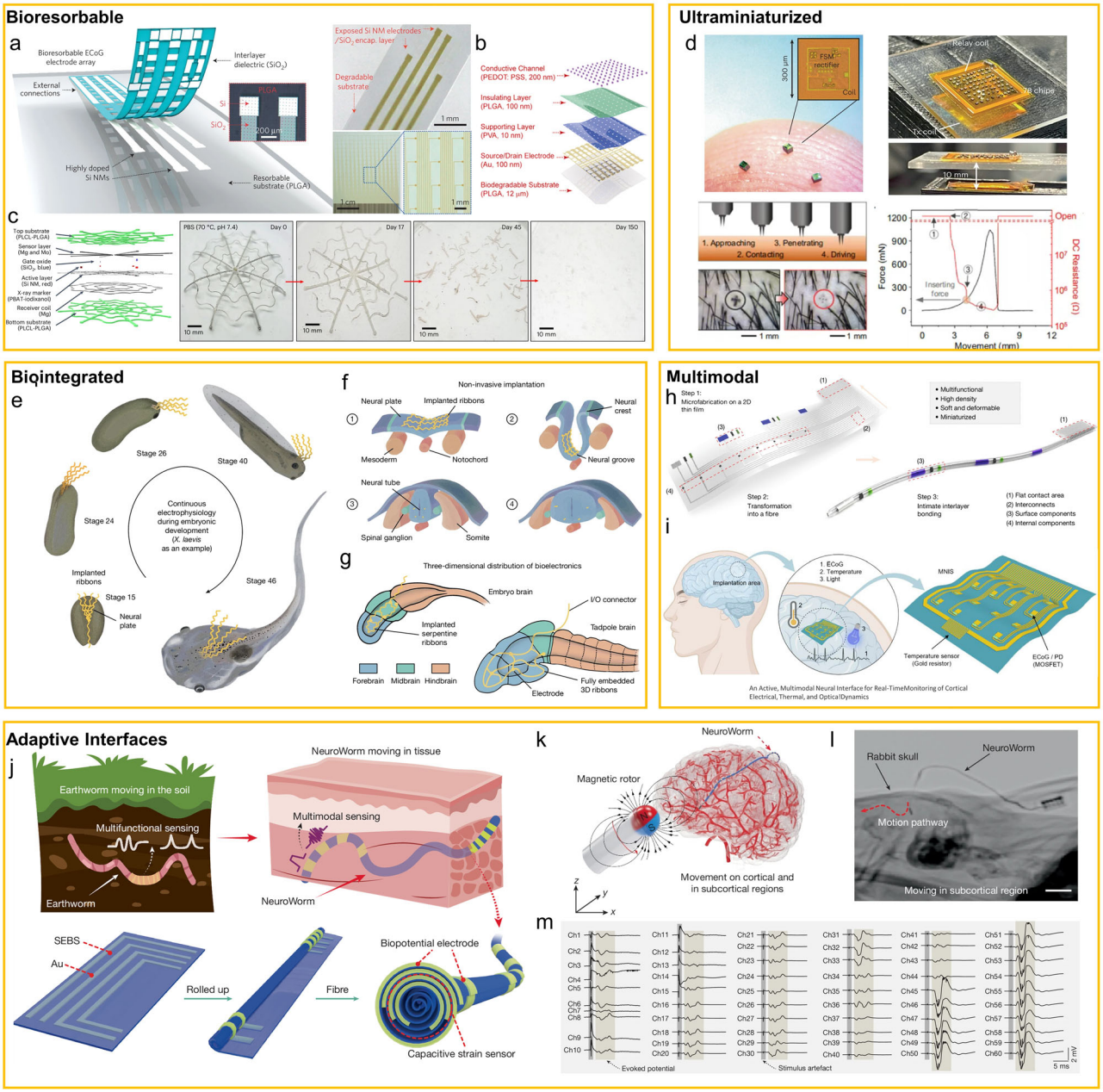

Fig. 6 | Frontier directions in neural interface devices and microsystems. a (left) Schematic exploded view illustration of the construction of a passive, bioresorbable neural electrode array for ECoG and sub-dermal EEG measurements, and a magnified optical image of electrodes on the right highlights the sensing (Si NMs) and insulating (SiO_2) regions. (right) Photographs of bioresorbable neural electrode arrays with 4 channels (top) and 256 (16 × 16 configuration) channels (bottom)[76] Copyright 2016, Springer Nature Ltd. **b** Schematic illustration showing a fully biodegradable, transient OECT platform engineered for high-spatiotemporal-resolution μ-ECoG recording. Copyright 2023, Wiley. **c** (left)Schematic exploded view (top) and photograph (bottom) of the biodegradable electronic tent with multifunctional electronic components. (right)Sequential dissolution images of the device immersed in 70 °C, pH 7.4 PBS for 150 d[118]. Copyright 2024, Springer Nature Ltd. **d** (up)Microphotograph of wireless ASIC prototype chips on a fingertip; Photo of benchtop three-coil antenna in wireless experiments[217]. Copyright 2024, Springer Nature Ltd. (Low) Schematic of microsensor insertion test in four stages: 1. Approaching, 2. Contacting, 3. Penetrating, 4. Driving[277]. Copyright 2025, PNAS. **e** The stepwise implantation of soft mesh electronics into the Xenopus embryo brain via organogenesis. **f** Schematics of coronal views of neural plate development. **g** Stretchable mesh electronics throughout the 3D structure of the brain[218]. Copyright 2025, Springer Nature Ltd. **h** Schematic of the morphological evolution from a 2D micropatterned film to a 1D fiber[94]. Copyright 2025, Springer Nature Ltd. **i** Architecture diagram of a multifunctional neural interface system enabling multimodal acquisition of cortical electrophysiology, temperature, and optical signals[224]. **j** Earthworm-inspired design concept and fabrication workflow of NeuroWorm. **k** Schematic depiction of NeuroWorm locomotion within the brain under magnetic guidance. **l** Demonstration of NeuroWorm movement in the rabbit subcortical region; scale bar, 1 cm. **m** Simultaneously recorded evoked CMAP signals by a single 60-channel fiber sensor during an acute experiment[225]. Copyright 2025, Springer Nature.

capable of recording cortical neural signals in mice without requiring surgical retrieval, and conductive polymer-based bioresorbable scaffolds such as PEDOT:PSS/PLLA that offer low-impedance tissue interfaces[211]. Furthermore, multilayer material systems such as Mg/PDLLA, Zn/PLA, and Fe/PLGA enable tunable degradation profiles to match distinct functional lifetimes. These advances not only demonstrate the feasibility of engineering transient neural interfaces with well-defined functional lifetimes but also point toward future systems in which degradation kinetics, mechanical

compliance, and microsystem-level functionality can be co-designed to achieve safer, smarter, and more adaptive brain-machine interfaces.

Injectable and deployable interfaces

Building on the limitations of conventional rigid brain-machine interfaces —such as insertion-induced tissue damage, large-scale displacement, and chronic immune responses—researchers have increasingly recognized that degradable materials alone cannot fully resolve the trade-off between minimal invasiveness and long-term stability. This realization has motivated a new class of injectable neural interfaces in which electronic devices remain in a mechanically robust, needle-like configuration during insertion, but spontaneously transform into soft, tissue-conformal structures once deployed in vivo. Such designs are enabled by ultrathin mesh architectures and stress-engineered self-rolling films, providing large-area, compliant interfaces that can be delivered through minimally invasive injection.

Syringe-injectable mesh electronics represent a seminal implementation of this design philosophy. Constructed from ~1 μm-thick SU-8/Au/Pt networks, these ultraflexible meshes can be compacted into a filament-like probe that fits within a ~100 μm-diameter needle and subsequently unfold inside the tissue to form a soft, tissue-modulus-matched interface[152]. This enables months-long electrophysiological recordings with remarkably low immune response. Building on this concept, the second-generation Mesh Electronics platform increased mesh density and functional site count, making it possible to achieve "injectable, single-cell-resolution arrays"[94]. A similar principle underlies the NeuroRoots architecture, in which 7 μm-diameter flexible microfibers are delivered through injection and then spontaneously spread and anchor within the brain parenchyma, mimicking natural axonal root structures[212]. This configuration supports stable, long-term single-unit recordings with minimal tissue disruption. Self-rolled biosensing interfaces and related developments extend this paradigm into three dimensions. By engineering multilayer films with tailored stress or residual-stress gradients, these systems undergo deployment-enabled structural transformation, rolling from planar 2D precursors into 3D self-rolled biosensor arrays (3D-SR-BAs) upon release of a sacrificial layer. Although not syringe-injectable themselves, the resulting cylindrical or tubular architectures illustrate how post-deployment 3D unfolding can generate conformal interfaces that wrap around biological tissues, enabling stable electrophysiological recording and integrated optical measurements within complex 3D geometries[213].

Further advances in materials engineering have enabled clinically safer and more comfortable approaches for injectable neural interfaces. Injectable neural interfaces often rely on deployment-enabled mechanical transformation, in which devices are delivered in a compact, mechanically stiff configuration and subsequently expand in situ to form soft, conformal electrical interfaces. An illustrative example is the self-deploying shape-memory-polymer (SMP) "tent" electrode shown in Fig. 6c. This device is fabricated from microscale-thick SMP films that can be folded into a compact structure with a diameter of less than 5 mm for implantation and then autonomously unfold in vivo triggered by a slight temperature increase to achieve nearly a 200-fold increase in surface area, enabling intimate tissue interfacing. Notably, when implemented using bioresorbable PLGA-based conductive composites, such deployable systems can further provide transient electrical functionality and subsequently dissolve on a programmable timescale, offering an additional advantage for temporary neural interfacing applications. This transformation is enabled by the reversible thermo-mechanical response of the SMP and the incorporation of deformable hinges, which together allow low-force, 3D deployment and conformal coverage across broad cortical regions. The platform also integrates a multiplexed electrode array and an NFC wireless module onto the same substrate, achieving ~12 dB SNR cortical recordings under fully wireless operation. With the exception of the NFC chip, all materials are bioresorbable, eliminating the need for device retrieval. Nonetheless, challenges remain. Because the SMP layer is only a few micrometers thick, its water-vapor permeability in vivo (10^{-14}–10^{-13} m^2 s^{-1}) leads to edge-seal delamination within 48–72 h, highlighting the gap between achieving reliable deployment and achieving long-term stable deployment. Overall, these "mesh/rolling-unfolding" electrode systems leverage extreme thinning, open-mesh geometries, and stress-driven self-assembly to reversibly transition between the compressed state required for injection and the expanded state required for functional interfacing within tissue[108].

In contrast to solid-state flexible electronics that rely on structural compression and in situ deployment, another class of injectable neural interfaces introduces materials into tissue in liquid or semi-fluid form, allowing them to self-assemble, gelate, or polymerize in the biofluid environment. This approach yields ultra-soft, tissue-modulus-matched conductive networks directly within the target region. A representative example is the PEDOT:PSS-based double-network conductive hydrogel[214], which remains flowable prior to injection but rapidly forms a highly conductive, ultra-soft gel electrode upon entering tissue, enabling a truly pressure-free electrical interface[215]. A representative example of liquid-state injectable interfaces relies on in situ polymerization, in which a mixture of conductive polymer precursors and oxidants is injected into tissue to spontaneously form a highly conductive polymer network within the local microenvironment. The EDOT-based system developed at the University of Tokyo exemplifies this strategy, eliminating the need for physical device implantation and thereby minimizing mechanical disturbance.

As material platforms continue to expand, MXene-hydrogel composite networks have emerged as promising candidates. Ti_3C_2 MXene sheets provide high electrical conductivity and support cryogelation-driven network formation, enabling conformal and stable electrical contacts after injection[216]. Silk-MXene conductive hydrogels similarly exist in a flowable state prior to injection and rapidly form a compliant, conductive 3D network in vivo, resulting in high-quality interfaces with surrounding neural tissue. Collectively, these examples highlight that the defining feature of injectable neural interfaces lies not in the delivery route alone, but in their ability to undergo deployment-enabled mechanical and structural transformation, enabling soft, conformal, and functionally integrated bioelectronic interfaces following minimally invasive implantation.

Ultraminiaturized and microscale interfaces

Conventional wireless implantable systems are fundamentally constrained in their ability to shrink below the millimeter scale due to the size requirements of electromagnetic antennas and the high tissue attenuation of RF signals. To overcome these limitations, a paradigm shift toward non-electromagnetic communication and power-delivery mechanisms has been proposed for ultraminiaturized neural interfaces. Neural dust represents a breakthrough toward ultra miniaturization by reducing the total device volume to the millimeter regime, with theoretical analyses suggesting the feasibility of scaling down to ~50 μm (Fig. 6d)[217].

The ultimate size limit is determined primarily by the lateral dimensions of the piezoelectric crystal and the signal-to-noise ratio of the ultrasonic backscatter communication link. The key enabler of this scaling trend is the use of a piezoelectric material as an "acoustic antenna," leveraging the low attenuation and short wavelength of ultrasound in biological tissue. This allows efficient energy coupling even at microscopic dimensions. Moreover, by employing passive backscatter modulation, the system eliminates the need for an onboard RF transmitter, thereby removing the power-hungry components, antennas, and driving circuits that traditionally dominate device size. However, several challenges emerge as the system shrinks. Reducing the piezoelectric crystal dimensions proportionally decreases the backscattered signal amplitude, rapidly degrading link SNR. Polymer encapsulation becomes susceptible to moisture permeation at micro-scale thicknesses, leading to early device failure. In addition, the angular sensitivity of piezoelectric particles relative to the external ultrasonic beam makes the communication link highly vulnerable to tissue micromotion (10–80 μm), which can disrupt alignment and stability. For these reasons, ultrasonic backscatter currently remains the only modality capable of combining wireless power delivery and bidirectional communication at micro-scale dimensions. Electromagnetic approaches require prohibitively high frequencies below the millimeter scale, resulting in severe tissue losses;

inductive coils suffer from drastically reduced coupling coefficients and tissue heating as they shrink; and optical schemes are fundamentally limited by penetration depth, making it difficult to establish a two-way link at comparable sizes. Looking forward, further advances in piezoelectric materials, encapsulation strategies, and adaptive ultrasonic interrogation schemes will be critical for pushing ultrasonic neural interfaces beyond current size and stability limits.

Long-term implantable interfaces

While transient and injectable interfaces address invasiveness and short-term compatibility, achieving truly long-term neural implantation remains an open frontier challenge due to persistent foreign body responses and tissue micromotion. One emerging strategy tackles this problem not by removing the device, but by rendering it mechanically invisible to the tissue through extreme softness and structural compliance, as demonstrated by PFPE-DMA ultraflexible mesh electrodes (Fig. 6e-g)[218].

PFPE-DMA represent a fundamentally different neural interface strategy -one that does not rely on bioresorption but instead achieves long-term biocompatibility through extreme mechanical compliance. By combining an ultra-low elastic modulus (approximately 10^4 times lower than that of conventional PI films) with submicron-thick serpentine interconnects (40 nm Cr/Au), the device attains tissue-matched flexibility that allows it to fold naturally with the tissue and embed within 3D structures. This unique property enables the electrode to conform to the developing neural plate of Xenopus embryos at stage 15, subsequently folding into the brain as the organism matures. The system supports single-cell-scale neural recording from embryonic stages to adulthood, and in regenerative models, it can track post-injury increases in activity as well as functional rewiring. Owing to the material's high chemical inertness and extremely low water absorption, the interface provokes minimal tissue irritation or inflammatory response over 30–60 days. Despite these advantages, several limitations remain. While the ultralow modulus provides exceptional compliance, it also reduces mechanical robustness in high-density interconnect layouts, with reliability decreasing notably when channel counts exceed 64. Moreover, extending this strategy to mammalian models is challenging, as such implants cannot be introduced through natural developmental folding processes, limiting the generalizability of this approach. Together, these ultraflexible, developmentally integrated interfaces highlight a frontier direction for long-term neural implantation in which chronic biocompatibility is achieved not through material resorption or replacement, but through mechanical invisibility, suggesting a complementary pathway toward lifelong neural interfaces when scalable deployment challenges can be addressed.

Multimodal neural interfaces

Recent years have witnessed rapid advances in multimodal neural interface technologies, driven by the growing recognition that single-modality measurements are insufficient to capture the complexity of neural circuit function.

Thermally drawn multifunctional fiber probes exemplify this progress[219]. Flexible fibers fabricated through the thermal drawing process can integrate neurotransmitter chemical sensing (e.g., fast-scan cyclic voltammetry), electrophysiological recording, optogenetic stimulation, and drug delivery within a single slender platform. This level of integration provides a powerful tool for probing synaptic-level neurochemical mechanisms in vivo. MRI-compatible multimodal fibers further expand experimental capabilities by combining low-loss optical waveguides, carbon-based conductors, and microelectrodes[220]. These probes enable simultaneous electrical, optical, and chemical interrogation in brain regions such as the mouse reward pathway, while remaining fully compatible with whole-brain imaging-substantially broadening their applicability in systems neuroscience.

In the domain of optical integration, implantable silicon photonic neural probes have demonstrated the ability to combine nanophotonic waveguides with microelectrode arrays, enabling optogenetic stimulation in deep-brain regions together with simultaneous electrophysiological recording[221]. Flexible, wireless micro-optoelectronic systems based on micro-LEDs further extend this capability by incorporating soft substrates and integrated light sources, providing stable chronic optical stimulation while reducing dependence on external optical fibers and bulky hardware[222]. Soft, transparent hydrogel or elastomer interfaces represent another route, emphasizing simultaneous optical and electrical access and offering a mechanically compliant platform for high-resolution deep-tissue imaging alongside electrochemical or electrophysiological sensing. As shown in Fig. 6h, a representative example employs 2D microfabricated SEBS/SBS elastomeric films that incorporate pressure sensors, electrochemical electrodes, electrophysiology sites, and optical waveguides patterned on and within the film using photolithography and laser-induced graphene (LIG) techniques. Through a self-adhering helical-wrapping process, these 2D films transform into 1D fiber devices with diameters of ~230–350 μm, preserving microscale patterns with high fidelity while reconfiguring the architecture into a 3D geometry. The tunable diameter and modulus of the thermoplastic elastomer scaffold enable co-integration of multimodal modules within a single fiber with low crosstalk (<5%), while maintaining stable adhesion and accommodating dynamic deformation within narrow luminal environments. In vivo studies demonstrate that these fibers can record continuous gastrointestinal motility for several days in the mouse colon and pig small intestine, and can maintain single-neuron-level recordings in the mouse hippocampus for up to four months with stable electrode impedance and SNR > 5[223]. With integrated optical waveguiding, the platform also supports localized optogenetic modulation, and histological analyses show minimal inflammatory response around the implant.

Beyond fiber- and fiber-like geometries, planar device architectures also enable deep multimodal integration, as exemplified by the multimodal neural interface system (MNIS) (Fig. 6i). Built on a flexible platform measuring approximately $3.28 \times 3.36\ mm^2$ and ~31 μm thick, the system incorporates electrical, thermal, and optical sensing within a 4×4 microarray, with each unit occupying a compact footprint of $220 \times 300\ \mu m^2$. A thermally grown SiO_2 insulating layer enables high-SNR neural signal acquisition through capacitive coupling, achieving up to 36.5 dB. Ultrathin metallic resistors provide cortical temperature measurements with 0.1 °C resolution, while PMOS photodetectors offer blue-light responsivities of ~0.55–0.57 nA $(mW{\cdot}cm^2)^{-1}$, enabling on-chip optical sensing without the need for separate photodiodes. Together, these components deliver spatially co-localized and structurally homogeneous tri-modal sensing within a single ultrathin platform. In vivo experiments in Sprague-Dawley rats demonstrate that MNIS can simultaneously and stably record ECoG signals, cortical temperature, and optical pulse stimuli. Temperature measurements show linear agreement with commercial thermocouples, and optical detection remains robust even at intensities as low as 0.02 $W{\cdot}m^{-2}$. Histological analyses reveal minimal tissue damage, with cell viability around 99%[224]. Such designs highlight the importance of synergistic materials engineering and structural co-integration in flexible multimodal neural interfaces, underscoring their potential for multi-signal coexistence and long-term stable recording. Collectively, these advances demonstrate that multimodal neural interfaces are transitioning from simple co-location of heterogeneous sensors toward deep, architecture-level integration in which electrical, optical, chemical, thermal, and mechanical functionalities are co-designed within unified platforms.

As a frontier direction, multimodal interfaces are increasingly enabling not only simultaneous observation of neural activity across multiple signal domains, but also causal interrogation through tightly coupled sensing, stimulation, and modulation at matched spatial and temporal scales.

Dynamic interfaces

Conventional neural electrodes are inherently static after implantation, limiting their ability to adapt to tissue deformation, target evolving regions of interest, or compensate for signal degradation over time. To address these constraints, an emerging frontier direction explores dynamic neural interfaces that incorporate controlled mobility within soft biological tissues, as exemplified by the NeuroWorm platform (Fig. 6j-m).

The NeuroWorm platform highlights a new class of flexible electrodes with dynamic mobility. By rolling ~400 nm-thick SEBS films into fibre-like structures, the system forms implantable sensors with diameters of ~109 μm that can incorporate up to 60 longitudinal electrode channels[225]. NeuroWorm is capable of simultaneously monitoring bioelectrical and mechanical signals. Its core innovation lies in its magnetically actuated mobility, which allows directional advancement through brain or muscle tissue to achieve dynamic, targeted signal acquisition—overcoming the traditional limitation that implanted electrodes must remain fixed and immobile. The extreme softness and stretchability of the fiber (stretch ratio~94%) enable it to conform to tissue deformation, thereby reducing immune response. In long-term rat muscle implantation studies (up to 43 weeks), NeuroWorm achieved stable electromyographic recordings with minimal fibrotic encapsulation (thickness <23 μm) and mild inflammatory response. In rabbit brain experiments, the fiber was able to move within cortical and subcortical regions while capturing high-quality electrophysiological signals. This emerging paradigm of dynamic electrode opens a new direction for flexible neural interfaces, transitioning from static placement to actively adjustable deployment. However, current open-loop magnetic actuation strategies remain limited in both locomotion speed and positioning accuracy. Future developments will require closed-loop control systems and large-scale electromagnetic coil arrays to enable more precise and safer navigation within biological tissues[226].

Taken together, the frontier directions outlined in this section reflect a fundamental shift in neural interface design. From static, monofunctional implants toward adaptive, multifunctional, and system-level platforms that more closely align with the mechanical, biological, and functional complexity of neural tissue. Rather than pursuing incremental improvements along a single dimension, recent advances increasingly emphasize co-design across materials, device architectures, and deployment strategies to overcome long-standing trade-offs between invasiveness, stability, scalability, and functionality[227].

Across bioresorbable, injectable, ultraminiaturized, long-term compliant, multimodal, and dynamic interfaces, a unifying theme emerges: future neural interfaces will not be defined solely by what they measure or stimulate, but by how they integrate, adapt, and interact with living systems over time. These approaches collectively point toward neural technologies that can be delivered with minimal disruption, operate reliably across extended timescales, and dynamically respond to evolving biological contexts.

Looking forward, translating these frontier concepts into broadly deployable clinical and research tools will require advances beyond individual device demonstrations, including scalable fabrication, closed-loop control, robust packaging, and standardized evaluation frameworks. As these challenges are addressed, the convergence of adaptability, multifunctionality, and long-term biocompatibility is poised to redefine the capabilities and roles of next-generation neural interfaces.

Conclusion and outlook

Brain-computer interfaces (BCIs) are advancing toward chronically implantable and clinically scalable systems, yet stable and high-efficiency neural recording remains fundamentally constrained by cross-level interactions. As discussed in this review, recording performance emerges from the coupled effects of electrode materials, device architectures, array configurations, and microsystem integration, rather than any single design element. Material properties define interfacial impedance, biocompatibility, and signal transduction mechanisms, while active devices and system architectures determine signal amplification, fidelity, and scalability. A key insight is that limitations at one level propagate across the system, underscoring that long-term stability is inherently a system-level co-design problem rather than an isolated materials or device challenge.

From a translational perspective, technologies that combine flexible electrode arrays with mature microelectronic integration are currently the most promising for near-term clinical deployment. These systems benefit from established fabrication processes, predictable performance, and demonstrated in vivo stability, making them well aligned with regulatory and industrialization pathways. In parallel, minimally invasive approaches, such as endovascular interfaces and ultraflexible probes, offer clear advantages in reducing surgical risk and improving patient compliance, although further validation of long-term reliability and safety is required. More broadly, successful clinical translation will depend not only on technical performance, but also on reproducibility, large-scale manufacturability, and standardized evaluation frameworks under chronic implantation conditions.

Looking ahead, emerging approaches, including organic and hybrid bioelectronic systems, mixed ionic-electronic materials, and neuromorphic interfaces, represent promising directions for long-term development. These strategies aim to achieve deeper integration with biological systems through mechanical compliance, volumetric signal transduction, and distributed signal processing. However, their translation will require advances in material stability, scalable fabrication, and system integration. Overall, future progress in BCIs will rely on cross-level integration, where materials, devices, and systems are co-optimized to enable robust, high-density, and long-lasting neural interfaces for clinical applications.

Data availability

No datasets were generated or analyzed during the current study.

Received: 26 January 2026; Accepted: 16 June 2026;
Published online: 29 June 2026

References

1. Zhang, H. et al. Brain-computer interfaces: the innovative key to unlocking neurological conditions. *Int. J. Surg.* **110**, 5745–5762 (2024).
2. Gulati, T. et al. Robust neuroprosthetic control from the stroke perilesional cortex. *J. Neurosci.* **35**, 8653–8661 (2015).
3. Donati, A. R. C. et al. Long-term training with a brain-machine interface-based gait protocol induces partial neurological recovery in paraplegic patients. *Sci. Rep.* **6**, 30383. https://doi.org/10.1038/srep30383 (2016).
4. Balasubramanian, K. et al. Changes in cortical network connectivity with long-term brain-machine interface exposure after chronic amputation. *Nat. Commun.* **8**, 1796 (2017).
5. Lebedev, M. A. & Nicolelis, M. A. Brain-machine interfaces: from basic science to neuroprostheses and neurorehabilitation. *Physiol. Rev.* **97**, 767–837 (2017).
6. Cervera, M. A. et al. Brain-computer interfaces for post-stroke motor rehabilitation: a meta-analysis. *Ann. Clin. Transl. Neurol.* **5**, 651–663 (2018).
7. Xie, Y.-L. et al. Brain-machine interface-based training for improving upper extremity function after stroke: a meta-analysis of randomized controlled trials. *Front. Neurosci.* **16**, 949575. https://doi.org/10.3389/fnins.2022.949575 (2022).
8. Liu, J. et al. Efficacy and safety of brain-computer interface for stroke rehabilitation: an overview of systematic review. *Front. Hum. Neurosci.* **19**, 1525293. https://doi.org/10.3389/fnhum.2025.1525293 (2025).
9. Biasiucci, A. et al. Brain-actuated functional electrical stimulation elicits lasting arm motor recovery after stroke. *Nat. Commun.* **9**, 2421 (2018).
10. Grosse-Wentrup, M., Mattia, D. & Oweiss, K. Using brain-computer interfaces to induce neural plasticity and restore function. *J. Neural Eng.* **8**, 025004 (2011).
11. Eliseyev, A. et al. Development of a brain-computer interface for patients in the critical care setting. *PLoS One* **16**, e0245540 (2021).
12. Canny, E. et al. Boosting brain-computer interfaces with functional electrical stimulation: potential applications in people with locked-in syndrome. *J. Neuroeng. Rehabil.* **20**, 157 (2023).

13. Neely, R. M. et al. Recent advances in neural dust: towards a neural interface platform. *Curr. Opin. Neurobiol.* **50**, 64–71 (2018).
14. Downey, J. E. et al. Intracortical recording stability in human brain-computer interface users. *J. Neural Eng.* **15**, 046016 (2018).
15. Nicolelis, M. A. L. & Lebedev, M. A. Principles of neural ensemble physiology underlying the operation of brain-machine interfaces. *Nat. Rev. Neurosci.* **10**, 530–540 (2009).
16. Seymour, J. P. et al. State-of-the-art MEMS and microsystem tools for brain research. *Microsyst. Nanoeng.* **3**, 16066. https://doi.org/10.1038/micronano.2016.66 (2017).
17. Song, E. et al. Materials for flexible bioelectronic systems as chronic neural interfaces. *Nat. Mater.* **19**, 590–603 (2020).
18. Lv, S. et al. Long-term stability strategies of deep brain flexible neural interface. *npj Flex. Electron.* **9**, 40 (2025).
19. Pimenta, S. et al. Flexible neural probes: a review of the current advantages, drawbacks, and future demands. *J. Zhejiang Univ. Sci. B* **25**, 153–167 (2024).
20. Agorelius, J. et al. An array of highly flexible electrodes with a tailored configuration locked by gelatin during implantation—initial evaluation in cortex cerebri of awake rats. *Front. Neurosci.* **9**, 331 (2015).
21. Irwin, Z. T. et al. Enabling low-power, multi-modal neural interfaces through a common, low-bandwidth feature space. *IEEE Trans. Neural Syst. Rehabil. Eng.* **24**, 521–531 (2015).
22. Harrison, R. R. et al. Wireless neural recording with single low-power integrated circuit. *IEEE Trans. Neural Syst. Rehabil. Eng.* **17**, 322–329 (2009).
23. Zhu, B. et al. Closed-loop neural prostheses with on-chip intelligence: a review and a low-latency machine learning model for brain state detection. *IEEE Trans. Biomed. Circuits Syst.* **15**, 877–897 (2021).
24. Chen, F.-D. et al. Implantable nanophotonic neural probes for integrated patterned photostimulation and electrophysiological recording. *npj Biosens.* **2**, 15 (2025).
25. Zhou, W. et al. Soft and stretchable organic bioelectronics for continuous intraoperative neurophysiological monitoring during microsurgery. *Nat. Biomed. Eng.* **7**, 1270–1281 (2023).
26. Liu, X. et al. Flexible high-density microelectrode arrays for closed-loop brain-machine interfaces: a review. *Front. Neurosci.* **18**, 1348434. https://doi.org/10.3389/fnins.2024.1348434 (2024).
27. Choi, J.-R. et al. Implantable neural probes for brain-machine interfaces: current developments and future prospects. *Exp. Neurobiol.* **27**, 453 (2018).
28. Ramesh, B. et al. Nontechnical loss detection using neural architecture search and outlier detection. *E3S Web Conf.* **256**, 01005 (2021).
29. Wu, N. et al. Electrode materials for brain-machine interface: a review. *InfoMat* **3**, 1174–1194 (2021).
30. Gao, W. et al. Revolutionizing brain–computer interfaces: overcoming biocompatibility challenges in implantable neural interfaces. *J. Nanobiotechnol.* **23**, 498 (2025).
31. Wang, K. et al. Clinical practice of brain-machine interfaces in neurological disorders. *Eng. Med.* **2**, 100090 (2025).
32. Slutzky, M. W. Brain-machine interfaces: powerful tools for clinical treatment and neuroscientific investigations. *Neuroscientist* **25**, 139–154 (2019).
33. Nair, D. R. et al. Nine-year prospective efficacy and safety of brain-responsive neurostimulation for focal epilepsy. *Neurology* **95**, e1244–e1256 (2020).
34. Bronte-Stewart, H. M. et al. Long-term personalized adaptive deep brain stimulation in Parkinson's disease: a nonrandomized clinical trial. *JAMA Neurol.* **82**, 1171–1180 (2025).
35. Scangos, K. W. et al. Closed-loop neuromodulation in an individual with treatment-resistant depression. *Nat. Med.* **27**, 1696–1700 (2021).
36. Sasaki, A. et al. Brain-controlled epidural stimulation restores corticospinal connectivity to improve upper-limb function in chronic tetraplegia. Preprint at: https://doi.org/10.1101/2025.07.02.25330433 (2025).
37. Metzger, S. L. et al. Highly generalizable spelling using a silent-speech BCI in a person with severe anarthria. *Brain-Computer Interface Research: A State-of-the-Art Summary.* Vol. **11**, 21–28 (Springer, 2024).
38. Littlejohn, K. T. et al. A streaming brain-to-voice neuroprosthesis to restore naturalistic communication. *Nat. Neurosci.* **28**, 902–912 (2025).
39. Bastian, L. et al. Closed-loop transcutaneous vagus nerve stimulation of sleep slow oscillations. *Brain Stimul* **18**, 241 (2025).
40. Deli, A. et al. Sleep stage can be selectively modulated through targeted deep-brain stimulation of brainstem circuits. *Brain Stimul.* **18**, 1931–1934 (2025).
41. Ang, K. K. & Guan, C. Brain-computer interface in stroke rehabilitation. *J. Comput. Sci. Eng.* **7**, 139–146 (2013).
42. Bretag, A. H. The glass micropipette electrode: a history of its inventors and users to 1950. *J. Gen. Physiol.* **149**, 417–430 (2017).
43. Hubel, D. H. Tungsten microelectrode for recording from single units. *Science* **125**, 549–550 (1957).
44. McNaughton, B. L. et al. The stereotrode: a new technique for simultaneous isolation of several single units in the central nervous system from multiple unit records. *J. Neurosci. Methods* **8**, 391–397 (1983).
45. O'Keefe, J. & Recce, M. L. Phase relationship between hippocampal place units and the EEG theta rhythm. *Hippocampus* **3**, 317–330 (1993).
46. Wise, K. D. et al. An integrated-circuit approach to extracellular microelectrodes. *IEEE Trans. Biomed. Eng.* **3**, 238–247 (1970).
47. Drake, K. L. et al. Performance of planar multisite microprobes in recording extracellular single-unit intracortical activity. *IEEE Trans. Biomed. Eng.* **35**, 719–732 (1988).
48. Barrese, J. et al. Failure mode analysis of silicon-based intracortical microelectrode arrays in non-human primates. *J. Neural Eng.* **10**, 066014 (2013).
49. Jun, J. J. et al. Fully integrated silicon probes for high-density recording of neural activity. *Nature.* **551**, 232–236 (2017).
50. Steinmetz, N. A. et al. Neuropixels 2.0: a miniaturized high-density probe for stable, long-term brain recordings. *Science* **372**, eabf4588. https://doi.org/10.1126/science.abf4588 (2021).
51. Rousche, P. J. et al. Flexible polyimide-based intracortical electrode arrays with bioactive capability. *IEEE Trans. Biomed. Eng.* **48**, 361–371 (2001).
52. Felix, S. H. et al. Insertion of flexible neural probes using rigid stiffeners attached with biodissolvable adhesive. *J. Vis. Exp.* **79**, e50609. https://doi.org/10.3791/50609 (2013).
53. Lee, K. et al. Flexible, scalable, high channel count stereo-electrode for recording in the human brain. *Nat. Commun.* **15**, 218 (2024).
54. Boran, E. et al. High-density ECoG improves the detection of high-frequency oscillations that predict seizure outcome. *Clin. Neurophysiol.* **130**, 1882–1888 (2019).
55. Swift, J. R. et al. Passive functional mapping of receptive language areas using electrocorticographic signals. *Clin. Neurophysiol.* **129**, 2517–2524 (2018).
56. Benabid, A. L. et al. An exoskeleton controlled by an epidural wireless brain-machine interface in a tetraplegic patient: a proof-of-concept demonstration. *Lancet Neurol.* **18**, 1112–1122 (2019).
57. Moly, A. et al. An adaptive closed-loop ECoG decoder for long-term and stable bimanual control of an exoskeleton by a tetraplegic. *J. Neural Eng.* **19**, 026014 (2022).
58. Anumanchipalli, G. K., Chartier, J. & Chang, E. F. Speech synthesis from neural decoding of spoken sentences. *Nature* **568**, 493–498 (2019).

59. Li, Y., Tang, C., Lu, J., Wu, J. & Chang, E. F. Human cortical encoding of pitch in tonal and non-tonal languages. *Nat. Commun.* **12**, 1161 (2021).
60. Hiremath, S. V. et al. Human perception of electrical stimulation on the surface of the somatosensory cortex. *PLoS One* **12**, e0176020 (2017).
61. Chen, X., Wang, F., Fernandez, E. & Roelfsema, P. R. Shape perception via a high-channel-count neuroprosthesis in monkey visual cortex. *Science* **370**, 1191–1196 (2020).
62. Beauchamp, M. S. et al. Dynamic stimulation of visual cortex produces form vision in sighted and blind humans. *Cell* **181**, 774–783.e775 (2020).
63. Leuthardt, E. C., Schalk, G., Wolpaw, J. R., Ojemann, J. G. & Moran, D. W. A brain-computer interface using electrocorticographic signals in humans. *J. Neural Eng.* **1**, 63–71 (2004).
64. Viventi, J. et al. Flexible, foldable, actively multiplexed, high-density electrode array for mapping brain activity in vivo. *Nat. Neurosci.* **14**, 1599–1605 (2011).
65. Yang, J. et al. Bacterial cellulose as a supersoft neural interfacing substrate. *ACS Appl. Mater. Interfaces* **10**, 33049–33059 (2018).
66. Tringides, C. M. et al. Viscoelastic surface electrode arrays to interface with viscoelastic tissues. *Nat. Nanotechnol.* **16**, 1019–1029 (2021).
67. Woods, V. et al. Long-term recording reliability of liquid crystal polymer μECoG arrays. *J. Neural Eng.* **15**, 066024 (2018).
68. Palma, M. et al. Chronic recording of cortical activity underlying vocalization in awake minipigs. *J. Neurosci. Methods* **366**, 109427. https://doi.org/10.1016/j.jneumeth.2021.109427 (2022).
69. Park, A. H. et al. Optogenetic mapping of functional connectivity in freely moving mice via insertable wrapping electrode array beneath the skull. *ACS Nano* **10**, 2791–2802 (2016).
70. Ji, B. et al. Flexible polyimide-based hybrid opto-electric neural interface with 16 channels of micro-LEDs and electrodes. *Microsyst. Nanoeng.* **4**, 27 (2018).
71. Kim, D. H. et al. Dissolvable films of silk fibroin for ultrathin conformal bio-integrated electronics. *Nat. Mater.* **9**, 511–517 (2010).
72. Thomas, C. A. Jr. et al. A miniature microelectrode array to monitor the bioelectric activity of cultured cells. *Exp. Cell Res.* **74**, 61–66 (1972).
73. Gross, G. W. Simultaneous single unit recording in vitro with a photoetched laser-deinsulated gold multimicroelectrode surface. *IEEE Trans. Biomed. Eng.* **5**, 273–279 (1979).
74. Maynard, E. M., Nordhausen, C. T. & Normann, R. A. The Utah intracortical electrode array: a recording structure for potential brain-computer interfaces. *Electroencephalogr. Clin. Neurophysiol.* **102**, 228–239 (1997).
75. Minev, I. R. et al. Electronic dura mater for long-term multimodal neural interfaces. *Science* **347**, 159–163 (2015).
76. Guan, S. et al. Elastocapillary self-assembled neurotassels for stable neural activity recordings. *Sci. Adv.* **5**, eaav2842. https://doi.org/10.1126/sciadv.aav2842 (2019).
77. Lee, J. M. et al. The ultra-thin, minimally invasive surface electrode array NeuroWeb for probing neural activity. *Nat. Commun.* **14**, 7088 (2023).
78. Musk, E. et al. An integrated brain-machine interface platform with thousands of channels. *J. Med. Internet Res.* **21**, e16194 (2019).
79. Woodington, B. J. et al. Flexible circumferential bioelectronics to enable 360-degree recording and stimulation of the spinal cord. *Sci. Adv.* **10**, eadl1230. https://doi.org/10.1126/sciadv.adl1230 (2024).
80. Xu, Y. et al. In-ear integrated sensor array for the continuous monitoring of brain activity and of lactate in sweat. *Nat. Biomed. Eng.* **7**, 1307–1320 (2023).
81. Liu, Y. et al. Soft conductive micropillar electrode arrays for biologically relevant electrophysiological recording. *Proc. Natl Acad. Sci. USA* **115**, 11718–11723 (2018).
82. Lee, S. H. et al. Scalable thousand channel penetrating microneedle arrays on flex for multimodal and large area coverage brain-machine interfaces. *Adv. Funct. Mater.* **32**, 2112045. https://doi.org/10.1002/adfm.202112045 (2022).
83. Adly, N. et al. Printed microelectrode arrays on soft materials: from PDMS to hydrogels. *npj Flex. Electron.* **2**, 15 (2018).
84. Grob, L. et al. Inkjet-printed and electroplated 3D electrodes for recording extracellular signals in cell culture. *Sensors* **21**, 3981 (2021).
85. Saleh, M. S. et al. CMU array: a 3D nanoprinted, fully customizable high-density microelectrode array platform. *Sci. Adv.* **8**, eabj4853. https://doi.org/10.1126/sciadv.abj4853 (2022).
86. Shin, H. et al. Multifunctional multi-shank neural probe for investigating and modulating long-range neural circuits in vivo. *Nat. Commun.* **10**, 3777 (2019).
87. Gu, Y. et al. Three-dimensional transistor arrays for intra- and inter-cellular recording. *Nat. Nanotechnol.* **17**, 292–300 (2022).
88. Chung, J. E. et al. High-density, long-lasting, and multi-region electrophysiological recordings using polymer electrode arrays. *Neuron* **101**, 21–31.e25 (2019).
89. Jiang, S. et al. Spatially expandable fiber-based probes as a multifunctional deep-brain interface. *Nat. Commun.* **11**, 6115 (2020).
90. Copeland, C. R. et al. Particle tracking of microelectromechanical system performance and reliability. *J. Microelectromech. Syst.* **27**, 948–950 (2018).
91. Park, Y. et al. Three-dimensional, multifunctional neural interfaces for cortical spheroids and engineered assembloids. *Sci. Adv.* **7**, eabf9153. https://doi.org/10.1126/sciadv.abf9153 (2021).
92. Abu Shihada, J. et al. Highly customizable 3D microelectrode arrays for in vitro and in vivo neuronal tissue recordings. *Adv. Sci.* **11**, e2305944. https://doi.org/10.1002/advs.202305944 (2024).
93. Lee, J. Y. et al. Foldable three-dimensional neural electrode arrays for simultaneous brain interfacing of cortical surface and intracortical multilayers. *npj Flex. Electron.* **6**, 86 (2022).
94. Zhou, T. et al. Syringe-injectable mesh electronics integrate seamlessly with minimal chronic immune response in the brain. *Proc. Natl Acad. Sci. USA.* **114**, 5894–5899 (2017).
95. Forbes, T. J. et al. Comparison of surgical, stent, and balloon angioplasty treatment of native coarctation of the aorta: an observational study by the CCISC (Congenital Cardiovascular Interventional Study Consortium). *J. Am. Coll. Cardiol.* **58**, 2664–2674 (2011).
96. Kolte, D. et al. Endovascular versus surgical revascularization for acute limb ischemia: a propensity-score matched analysis. *Circ. Cardiovasc. Interv.* **13**, e008150. https://doi.org/10.1161/circinterventions.119.008150 (2020).
97. Mitchell, P. et al. Assessment of safety of a fully implanted endovascular brain-computer interface for severe paralysis in 4 patients: the Stentrode with thought-controlled digital switch (SWITCH) study. *JAMA Neurol.* **80**, 270–278 (2023).
98. Thielen, B. et al. Making a case for endovascular approaches for neural recording and stimulation. *J. Neural Eng.* **20**, 016001 (2023).
99. Lylyk, P. et al. First-in-human endovascular treatment of hydrocephalus with a miniature biomimetic transdural shunt. *J. Neurointerv. Surg.* **14**, 495–499 (2022).
100. Yaeger, K. & Mocco, J. Future directions of endovascular neurosurgery. *Neurosurg. Clin. N. Am.* **33**, 233–239 (2022).
101. Wang, X. et al. Intravascular delivery of an ultraflexible neural electrode array for recordings of cortical spiking activity. *Nat. Commun.* **15**, 9442 (2024).

102. Li, H., Wang, J. & Fang, Y. Recent developments in multifunctional neural probes for simultaneous neural recording and modulation. *Microsyst. Nanoeng.* **9**, 4 (2023).
103. Winter-Hjelm, N. et al. Nanoporous platinum microelectrode arrays for neuroscience applications. *RSC Adv.* **15**, 5822–5836 (2025).
104. Schelles, M. et al. Optimization of sputtered iridium oxide microelectrodes for long-term intracortical stimulation. *Biomed. Phys. Eng. Express* **11**, 045012 (2025).
105. Kim, Y. H. et al. In vitro extracellular recording and stimulation performance of nanoporous gold-modified multi-electrode arrays. *J. Neural Eng.* **12**, 066029 (2015).
106. Goncalves, S. B., Peixoto, A. C., Rodrigues, J. A., Silva, A. F. & Correia, J. H. Microshaping of aluminum-based neural microelectrode arrays using chemical wet-etching. *Procedia Eng.* **87**, 939–942 (2014).
107. Guo, C. F. et al. Fatigue-free, superstretchable, transparent, and biocompatible metal electrodes. *Proc. Natl. Acad. Sci. USA* **112**, 12332–12337 (2015).
108. Shah Idil, A. & Donaldson, N. The use of tungsten as a chronically implanted material. *J. Neural Eng.* **15**, 021006 (2018).
109. Dollt, M. et al. Low-temperature atomic layer deposited oxide on titanium nitride electrodes enables culture and physiological recording of electrogenic cells. *Front. Neurosci.* **14**, 552876. https://doi.org/10.3389/fnins.2020.552876 (2020).
110. Sankar, V. et al. Electrode impedance analysis of chronic tungsten microwire neural implants: understanding abiotic vs. biotic contributions. *Front. Neuroeng.* **7**, 13 (2014).
111. Fiáth, R. et al. A silicon-based neural probe with densely-packed low-impedance titanium nitride microelectrodes for ultrahigh-resolution in vivo recordings. *Biosens. Bioelectron.* **106**, 86–92 (2018).
112. Li, J. et al. Sensing and stimulation applications of carbon nanomaterials in implantable brain-computer interface. *Int. J. Mol. Sci.* **24**, 5182 (2023).
113. Yuan, M. et al. Transparent, flexible graphene-ITO-based neural microelectrodes for simultaneous electrophysiology recording and calcium imaging of intracortical neural activity in freely moving mice. *Microsyst. Nanoeng.* **11**, 32 (2025).
114. Wei, W. & Wang, X. Graphene-based electrode materials for neural activity detection. *Materials* **14**, 6170 (2021).
115. Yuk, H., Lu, B. & Zhao, X. Hydrogel bioelectronics. *Chem. Soc. Rev.* **48**, 1642–1667 (2019).
116. Uz, M. & Mallapragada, S. K. Conductive polymers and hydrogels for neural tissue engineering. *J. Indian Inst. Sci.* **99**, 489–510 (2019).
117. Wang, F., Ma, M., Fu, R. & Zhang, X. EEG-based detection of driving fatigue using a novel electrode. *Sens. Actuators A Phys.* **365**, 114895. https://doi.org/10.1016/j.sna.2023.114895 (2024).
118. Bae, J.-Y. et al. A biodegradable and self-deployable electronic tent electrode for brain cortex interfacing. *Nat. Electron.* **7**, 815–828 (2024).
119. Khang, D.-Y., Jiang, H., Huang, Y. & Rogers, J. A. A stretchable form of single-crystal silicon for high-performance electronics on rubber substrates. *Science* **311**, 208–212 (2006).
120. Huang, X. et al. Fully biodegradable and long-term operational primary zinc batteries as power sources for electronic medicine. *ACS Nano* **17**, 5727–5739 (2023).
121. Kim, D.-H. et al. Epidermal electronics. *Science* **333**, 838–843 (2011).
122. Song, E. et al. Ultrathin trilayer assemblies as long-lived barriers against water and ion penetration in flexible bioelectronic systems. *ACS Nano* **12**, 10317–10326 (2018).
123. Fujishiro, A., Kaneko, H., Kawashima, T., Ishida, M. & Kawano, T. In vivo neuronal action potential recordings via three-dimensional microscale needle-electrode arrays. *Sci. Rep.* **4**, 4868 (2014).
124. Shao, Y. et al. Multi-functional, conformal systems with ultrathin crystalline-silicon-based bioelectronics for characterization of intraocular pressure and ocular surface temperature. *Biosens. Bioelectron.* **267**, 116786. https://doi.org/10.1016/j.bios.2024.116786 (2025).
125. Roisin, N. et al. Phonon-limited mobility for electrons and holes in highly-strained silicon. *npj Comput. Mater.* **10**, 242 (2024).
126. Sengupta, K., Nagatsuma, T. & Mittleman, D. M. Terahertz integrated electronic and hybrid electronic-photonic systems. *Nat. Electron.* **1**, 622–635 (2018).
127. Zhang, F. et al. Multimodal electrocorticogram active electrode array based on zinc oxide-thin film transistors. *Adv. Sci.* **10**, e2204467. https://doi.org/10.1002/advs.202204467 (2023).
128. Xie, P. et al. Solution-processed ultra-flexible C8-BTBT organic thin-film transistors with the corrected mobility over 18 $cm^2 V^{-1} s^{-1}$. *Sci. Bull.* **65**, 791–795 (2020).
129. Sawamoto, M., Sugino, H., Nakano, M. & Takimiya, K. High-performance solution-processed organic thin-film transistors based on a soluble DNTT derivative. *Org. Electron.* **46**, 68–76 (2017).
130. Kneppe, D. et al. Solution-processed pseudo-vertical organic transistors based on TIPS-pentacene. *Mater. Today Energy* **21**, 100697. https://doi.org/10.1016/j.mtener.2021.100697 (2021).
131. Wang, Y. et al. A highly stretchable, transparent, and conductive polymer. *Sci. Adv.* **3**, e1602076. https://doi.org/10.1126/sciadv.1602076 (2017).
132. Liu, Y. et al. Author correction: morphing electronics enable neuromodulation in growing tissue. *Nat. Biotechnol.* **38**, 1097 (2020).
133. Li, J. et al. A tissue-like neurotransmitter sensor for the brain and gut. *Nature* **606**, 94–101 (2022).
134. Wang, W. et al. Neuromorphic sensorimotor loop embodied by monolithically integrated, low-voltage, soft e-skin. *Science* **380**, 735–742 (2023).
135. Huang, J. et al. Electrochemical exfoliation of pillared-layer metal-organic framework to boost the oxygen evolution reaction. *Angew. Chem. Int. Ed.* **130**, 4722–4726 (2018).
136. Wang, X. et al. Ultraflexible PEDOT:PSS/IrOx-modified electrodes: applications in behavioral modulation and neural signal recording in mice. *Micromachines* **15**, 447 (2024).
137. Wang, A., Jung, D., Lee, D. & Wang, H. Impedance characterization and modeling of subcellular to micro-sized electrodes with varying materials and PEDOT:PSS coating for bioelectrical interfaces. *ACS Appl. Electron. Mater.* **3**, 5226–5239 (2021).
138. Bianchi, M. et al. Poly(3,4-ethylenedioxythiophene)-based neural interfaces for recording and stimulation: fundamental aspects and in vivo applications. *Adv. Sci.* **9**, e2104701. https://doi.org/10.1002/advs.202104701 (2022).
139. Kim, H. W. et al. Transparent, metal-free PEDOT:PSS neural interfaces for simultaneous recording of low-noise electrophysiology and artifact-free two-photon imaging. *Nat. Commun.* **16**, 4032 (2025).
140. Cuttaz, E. A. et al. Stretchable, fully polymeric electrode arrays for peripheral nerve stimulation. *Adv. Sci.* **8**, 2004033. https://doi.org/10.1002/advs.202004033 (2021).
141. Jiang, Y. et al. Topological supramolecular network enabled high-conductivity, stretchable organic bioelectronics. *Science* **375**, 1411–1417 (2022).
142. Cui, X. & Martin, D. C. Electrochemical deposition and characterization of poly (3, 4-ethylenedioxythiophene) on neural microelectrode arrays. *Sens. Actuators B Chem.* **89**, 92–102 (2003).
143. Kozai, T. et al. Ultrasmall implantable composite microelectrodes with bioactive surfaces for chronic neural interfaces. *Nat. Mater.* **11**, 1065–1073 (2012).
144. Liu, Y. et al. Soft and elastic hydrogel-based microelectronics for localized low-voltage neuromodulation. *Nat. Biomed. Eng.* **3**, 58–68 (2019).

145. Zhao, Z. et al. Ultraflexible electrode arrays for months-long high-density electrophysiological mapping of thousands of neurons in rodents. *Nat. Biomed. Eng.* **7**, 520–532 (2023).
146. RoaFiore, L. et al. Label-free functional imaging of vagus nerve stimulation-evoked potentials at the cortical surface. *npj Biosensing* **1**, 11 (2024).
147. Sepehri Rad, M. et al. Voltage and calcium imaging of brain activity. *Biophys. J.* **113**, 2160–2167 (2017).
148. Karadas, M. et al. In-vitro recordings of neural magnetic activity from the auditory brainstem using color centers in diamond: a simulation study. *Front. Neurosci.* **15**, 643614. https://doi.org/10.3389/fnins.2021.643614 (2021).
149. Herreras, O. Local field potentials: myths and misunderstandings. *Front. Neural Circuits* **10**, 101 (2016).
150. Sodagar, A. M., Khazaei, Y., Nekoui, M. & Shaeri, M. Real-time neural signal processing for high-density brain-implantable devices. *Bioelectron. Med.* **11**, 17 (2025).
151. Cheng, J., Xiao, M. & Li, Z. Structural and functional designs of advanced neural electrodes. *ACS Appl. Mater. Interfaces* **17**, 59010–59031 (2025).
152. Lin, C. et al. Flexible carbon nanotubes electrode for neural recording. *Biosens. Bioelectron.* **24**, 2791–2797 (2009).
153. Alahi, M. E. E. et al. Recent advancements in graphene-based implantable electrodes for neural recording/stimulation. *Sensors* **23**, 9911 (2023).
154. Khodagholy, D. et al. NeuroGrid: recording action potentials from the surface of the brain. *Nat. Neurosci.* **18**, 310–315 (2015).
155. Fang, H. et al. Capacitively coupled arrays of multiplexed flexible silicon transistors for long-term cardiac electrophysiology. *Nat. Biomed. Eng.* **1**, 0038. https://doi.org/10.1038/s41551-017-0038 (2017).
156. Chiang, C.-H. et al. Development of a neural interface for high-definition, long-term recording in rodents and nonhuman primates. *Sci. Transl. Med.* **12**, eaay4682. https://doi.org/10.1126/scitranslmed.aay4682 (2020).
157. Lewis, C. M. et al. Recording quality is systematically related to electrode impedance. *Adv. Healthc. Mater.* **13**, e2303401. https://doi.org/10.1002/adhm.202303401 (2024).
158. Park, H., Takmakov, P. & Lee, H. Electrochemical evaluations of fractal microelectrodes for energy efficient neurostimulation. *Sci. Rep.* **8**, 4375 (2018).
159. Li, J. et al. Conductively coupled flexible silicon electronic systems for chronic neural electrophysiology. *Proc. Natl. Acad. Sci. USA.* **115**, E9542–E9549 (2018).
160. Ohayon, D., Druet, V. & Inal, S. A guide for the characterization of organic electrochemical transistors and channel materials. *Chem. Soc. Rev.* **52**, 1001–1023 (2023).
161. Cogan, S. F. Neural stimulation and recording electrodes. *Annu. Rev. Biomed. Eng.* **10**, 275–309 (2008).
162. Lago, N. & Cester, A. Flexible and organic neural interfaces: a review. *Appl. Sci* **7**, 1292 (2017).
163. Rivnay, J. et al. Organic electrochemical transistors. *Nat. Rev. Mater.* **3**, 17086. https://doi.org/10.1038/natrevmats.2017.86 (2018).
164. Alahi, M. E. E. et al. Recent advancement of electrocorticography (ECoG) electrodes for chronic neural recording/stimulation. *Mater. Today Commun.* **29**, 102853. https://doi.org/10.1016/j.mtcomm.2021.102853 (2021).
165. Wei, S. et al. Shape-changing electrode array for minimally invasive large-scale intracranial brain activity mapping. *Nat. Commun.* **15**, 715 (2024).
166. Harrison, R. R. The design of integrated circuits to observe brain activity. *Proc. IEEE* **96**, 1203–1216 (2008).
167. Moosaei, A., Maghami, M. H., Nejati, A., Amiri, P. & Sawan, M. A low-power, low-noise recycling folded-cascode operational transconductance amplifier for neural recording applications. *Electronics* **14**, 1543 (2025).
168. Ng, K. A., Greenwald, E., Xu, Y. P. & Thakor, N. V. Implantable neurotechnologies: a review of integrated circuit neural amplifiers. *Med. Biol. Eng. Comput.* **54**, 45–62 (2016).
169. Tasneem, N. T. & Mahbub, I. A 2.53 NEF 8-bit 10 kS/s 0.5 µm CMOS neural recording read-out circuit with high linearity for neuromodulation implants. *Electronics* **10**, 590 (2021).
170. Mohtashamnia, M. & Yavari, M. A closed-loop neural recording analog front-end with low noise and automatic gain control amplifiers. *AEU Int. J. Electron. Commun.* **201**, 155976. https://doi.org/10.1016/j.aeue.2025.155976 (2025).
171. Ranjbar Koleibi, E. et al. Design and implementation of a low-power biopotential amplifier in 28 nm CMOS technology with a compact die-area of 2500 µm2 and an ultra-high input impedance. *Sensors* **25**, 2320 (2025).
172. Zhang, S. et al. Strain-controlled power devices as inspired by human reflex. *Nat. Commun.* **11**, 326 (2020).
173. Huang, W. et al. Vertical organic electrochemical transistors for complementary circuits. *Nature* **613**, 496–502 (2023).
174. Wu, M. et al. Ultrathin, soft, bioresorbable organic electrochemical transistors for transient spatiotemporal mapping of brain activity. *Adv. Sci.* **10**, 2300504. https://doi.org/10.1002/advs.202300504 (2023).
175. Shukla, G., Bisht, R. S. & Kumar, P. Predicting the miniaturization limit of vertical organic field effect transistor (VOFET) with perforated graphene as a source electrode. *Nanotechnology* **35**, 035201 (2023).
176. Polikov, V. S., Tresco, P. A. & Reichert, W. M. Response of brain tissue to chronically implanted neural electrodes. *J. Neurosci. Methods* **148**, 1–18 (2005).
177. Fu, T. M. et al. Stable long-term chronic brain mapping at the single-neuron level. *Nat. Methods* **13**, 875–882 (2016).
178. Einevoll, G. T., Franke, F., Hagen, E., Pouzat, C. & Harris, K. D. Towards reliable spike-train recordings from thousands of neurons with multielectrodes. *Curr. Opin. Neurobiol.* **22**, 11–17 (2012).
179. Tsai, D., Sawyer, D., Bradd, A., Yuste, R. & Shepard, K. L. A very large-scale microelectrode array for cellular-resolution electrophysiology. *Nat. Commun.* **8**, 1802 (2017).
180. Pérez-Prieto, N. & Delgado-Restituto, M. Recording strategies for high channel count, densely spaced microelectrode arrays. *Front. Neurosci.* **15**, 681085. https://doi.org/10.3389/fnins.2021.681085 (2021).
181. Zhou, E. et al. Chronically stable, high-resolution micro-electrocorticographic brain-computer interfaces for real-time motor decoding. *Adv. Sci.* **12**, e06663. https://doi.org/10.1002/advs.202506663 (2025).
182. Xie, Y. et al. High-resolution spatial mapping of electrocorticographic activities with NeuroCam: a 4096-channel, multiplexed flexible thin-film transistor array. *Sci. Bull.* **70**, 4133–4137 (2025).
183. Tchoe, Y. et al. Human brain mapping with multithousand-channel PtNRGrids resolves spatiotemporal dynamics. *Sci. Transl. Med.* **14**, eabj1441. https://doi.org/10.1126/scitranslmed.abj1441 (2022).
184. Guan, S. et al. Self-assembled ultraflexible probes for long-term neural recordings and neuromodulation. *Nat. Protoc.* **18**, 1712–1744 (2023).
185. Liu, Y. et al. A high-density 1,024-channel probe for brain-wide recordings in non-human primates. *Nat. Neurosci.* **27**, 1620–1631 (2024).
186. Zhao, Y., Tang, L., Rennaker, R., Hutchens, C. & Ibrahim, T. S. Studies in RF power communication, SAR, and temperature elevation in wireless implantable neural interfaces. *PLoS One* **8**, e77759 (2013).

187. Kim, S., Tathireddy, P., Normann, R. A. & Solzbacher, F. Thermal impact of an active 3-D microelectrode array implanted in the brain. *IEEE Trans. Neural Syst. Rehabil. Eng.* **15**, 493–501 (2007).
188. Wolf, P. D. Thermal considerations for the design of an implanted cortical brain–machine interface (BMI). **3** (Reichert W. M., 2008).
189. Whalen, A. J. et al. Thermal safety considerations for implantable micro-coil design. *J. Neural Eng.* **20**, 046017 (2023).
190. Obaid, A. et al. Massively parallel microwire arrays integrated with CMOS chips for neural recording. *Nat. Biomed. Eng*. **12**; https://doi.org/10.1126/sciadv.aay2789 (2020).
191. Yang, J., Zhao, S., Wang, J., Lin, S., Hou, Q. & Sawan, M. Precise and low-power closed-loop neuromodulation through algorithm-integrated circuit co-design. *Front. Neurosci.* **18**, 1340164. https://doi.org/10.3389/fnins.2024.1340164 (2024).
192. He, Y. et al. An event-based neural compressive telemetry with >11× loss-less data reduction for high-bandwidth intracortical brain computer interfaces. *IEEE Trans. Biomed. Circuits Syst.* **18**, 1100–1111 (2024).
193. Wang, Y., Ge, M. & Xu, S. Advances in brain-computer interfaces (BCI): challenges and opportunities. *Biomimetics* **11**, 157 (2026).
194. Jung, T. et al. A Wireless subdural-contained brain-computer interface with 65,536 electrodes and 1024 channels. *Nat. Electron.* **8**, 1272–1288 (2025).
195. Araki, T. et al. Flexible neural interfaces for brain implants—the pursuit of thinness and high density. *Flexible Printed Electron* **5**, 043002 (2020).
196. Lanzio, V. et al. High-density electrical and optical probes for neural readout and light focusing in deep brain tissue. *J. Micro/Nanolith. MEMS MOEMS* **17**, 025503 (2018).
197. Wei, X. et al. Nanofabricated ultraflexible electrode arrays for high-density intracortical recording. *Adv. Sci.* **5**, 1700625. https://doi.org/10.1002/advs.201700625 (2018).
198. Luan, L. et al. Ultraflexible nanoelectronic probes form reliable, glial scar-free neural integration. *Sci. Adv.* **3**, e1601966 (2017).
199. Stevenson, I. & Kording, K. How advances in neural recording affect data analysis. *Nat. Neurosci.* **14**, 139–142 (2011).
200. Ouyang, W. et al. A wireless and battery-less implant for multimodal closed-loop neuromodulation in small animals. *Nat. Biomed. Eng.* **7**, 1252–1269 (2023).
201. Chen, J. C. et al. Endocisternal interfaces for minimally invasive neural stimulation and recording of the brain and spinal cord. *Nat. Biomed. Eng.* **9**, 896–904 (2025).
202. Oxley, T. J. et al. Minimally invasive endovascular stent-electrode array for high-fidelity, chronic recordings of cortical neural activity. *Nat. Biotechnol.* **34**, 320–327 (2016).
203. Trautmann, E. M. et al. Large-scale high-density brain-wide neural recording in nonhuman primates. *Nat. Neurosci.* **28**, 1562–1575 (2025).
204. Wairagkar, M. et al. An instantaneous voice-synthesis neuroprosthesis. *Nature* **644**, 145–152 (2025).
205. Hwang, S.-W. et al. A physically transient form of silicon electronics. *Science* **337**, 1640–1644 (2012).
206. Yu, K. J. et al. Bioresorbable silicon electronics for transient spatiotemporal mapping of electrical activity from the cerebral cortex. *Nat. Mater.* **15**, 782–791 (2016).
207. Kang, S. K., Murphy, R., Hwang, S. W. et al. Bioresorbable silicon electronic sensors for the brain. *Nature* **530**, 71–76 (2016).
208. Hjort, M. et al. In situ assembly of bioresorbable organic bioelectronics in the brain. *Nat. Commun.* **14**, 4453 (2023).
209. Tang, H. et al. Injectable ultrasonic sensor for wireless monitoring of intracranial signals. *Nature* **630**, 84–90 (2024).
210. Khandelwal, A. et al. Self-assembled microtubular electrodes for on-chip low-voltage electrophoretic manipulation of charged particles and macromolecules. *Microsyst. Nanoeng.* **8**, 27 (2022).
211. Zhang, C. et al. Magnesium-based biodegradable microelectrodes for neural recording. *Mater. Sci. Eng. C* **110**, 110614. https://doi.org/10.1016/j.msec.2019.110614 (2020).
212. Ferro, M. D. et al. NeuroRoots, a bio-inspired, seamless brain machine interface for long-term recording in delicate brain regions. *AIP Adv.* **14**, 085109. https://doi.org/10.1063/5.0216979 (2024).
213. Kalmykov, A. et al. Organ-on-a-chip: three-dimensional self-rolled biosensor array for electrical interrogations of human electrogenic spheroids. *Sci. Adv.* **5**, eaax0729. https://doi.org/10.1126/sciadv.aax0729 (2019).
214. Kusen, I. et al. Injectable conductive hydrogel electrodes for minimally invasive neural interfaces. *J. Mater. Chem. B* **12**, 8929–8940 (2024).
215. Murbach, J. M. et al. In situ electrochemical polymerization of poly(3,4-ethylenedioxythiophene) (PEDOT) for peripheral nerve interfaces. *MRS Commun.* **8**, 1043–1049 (2018).
216. Zhang, Z. et al. Ti3C2Tx MXene composite 3D hydrogel potentiates mTOR signaling to promote the generation of functional hair cells in cochlea organoids. *Adv. Sci.* **9**, e2203557. https://doi.org/10.1002/advs.202203557 (2022).
217. Lee, J. et al. An asynchronous wireless network for capturing event-driven data from large populations of autonomous sensors. *Nat. Electron.* **7**, 313–324 (2024).
218. Sheng, H. et al. Brain implantation of soft bioelectronics via embryonic development. *Nature* **642**, 954–964 (2025).
219. Kim, Y. et al. Multifunctional and flexible neural probe with thermally drawn fibers for bidirectional synaptic probing in the brain. *ACS Nano* **18**, 13277–13285 (2024).
220. Antonini, M. J. et al. Customizing MRI-compatible multifunctional neural interfaces through fiber drawing. *Adv. Funct. Mater.* **31**, 2104857. https://doi.org/10.1002/adfm.202104857 (2021).
221. Chen, F. D. et al. Implantable silicon neural probes with nanophotonic phased arrays for single-lobe beam steering. *Commun. Eng.* **3**, 182 (2024).
222. Park, S. I. et al. Soft, stretchable, fully implantable miniaturized optoelectronic systems for wireless optogenetics. *Nat. Biotechnol.* **33**, 1280–1286 (2015).
223. Khatib, M. et al. High-density soft bioelectronic fibres for multimodal sensing and stimulation. *Nature* **645**, 656–664 (2025).
224. Li, J. et al. An active, multimodal neural interface for real-time monitoring of cortical electrical, thermal, and optical dynamics. *Adv. Sci.* **13**, e202512114. https://doi.org/10.1002/advs.202512114 (2025).
225. Xie, R. et al. A movable long-term implantable soft microfibre for dynamic bioelectronics. *Nature* **645**, 648–655 (2025).
226. Jiang, J., Yang, L. & Zhang, L. Closed-loop control of a Helmholtz coil system for accurate actuation of magnetic microrobot swarms. *IEEE Robot. Autom. Lett.* **6**, 827–834 (2021).
227. Laiwalla, F., & Nurmikko, A. Future of neural interfaces. *Neural Interface: Frontiers and Applications* **1101**, 225–241 (Springer, 2019).
228. Xu, L. et al. Trends and recent development of the microelectrode arrays (MEAs). *Biosens. Bioelectron.* **175**, 112854. https://doi.org/10.1016/j.bios.2020.112854 (2021).
229. Raman, J., Ishikawa, S., Storer, M. M. & Power, J. M. Surgical radiofrequency ablation of both atria for atrial fibrillation: results of a multicenter trial. *J. Thorac. Cardiovasc. Surg.* **126**, 1357–1366 (2003).
230. Pessiglione, M. et al. Thalamic neuronal activity in dopamine-depleted primates: evidence for a loss of functional segregation within basal ganglia circuits. *J. Neurosci.* **25**, 1523–1531 (2005).
231. Lapatki, B. G., Van Dijk, J. P., Jonas, I. E., Zwarts, M. J. & Stegeman, D. F. A thin, flexible multielectrode grid for high-density surface EMG. *J. Appl. Physiol.* **96**, 327–336 (2004).

232. Colnat-Coulbois, S. et al. Bilateral subthalamic nucleus stimulation improves balance control in Parkinson's disease. *J. Neurol. Neurosurg. Psychiatry* **76**, 780–787 (2005).
233. Cheung, K. C., Renaud, P., Tanila, H. & Djupsund, K. Flexible polyimide microelectrode array for in vivo recordings and current source density analysis. *Biosens. Bioelectron.* **22**, 1783–1790 (2007).
234. Butson, C. R., Cooper, S. E., Henderson, J. M. & McIntyre, C. C. Patient-specific analysis of the volume of tissue activated during deep brain stimulation. *NeuroImage* **34**, 661–670 (2007).
235. Wang, K., Liu, C. C. & Durand, D. M. Flexible nerve stimulation electrode with iridium oxide sputtered on liquid crystal polymer. *IEEE Trans. Biomed. Eng.* **56**, 6–14 (2009).
236. Viventi, J. et al. A conformal, bio-interfaced class of silicon electronics for mapping cardiac electrophysiology. *Sci. Transl. Med.* **2**, 24ra22 (2010).
237. Guitchounts, G., Markowitz, J. E., Liberti, W. A. & Gardner, T. J. A carbon-fiber electrode array for long-term neural recording. *J. Neural Eng.* **10**, 046016 (2013).
238. Kang, M. et al. Subcellular neural probes from single-crystal gold nanowires. *ACS Nano* **8**, 8182–8189 (2014).
239. Nelson, B. J., Kaliakatsos, I. K. & Abbott, J. J. Microrobots for minimally invasive medicine. *Annu. Rev. Biomed. Eng.* **12**, 55–85 (2010).
240. Liu, J. et al. Syringe-injectable electronics. *Nat. Nanotechnol.* **10**, 629–636 (2015).
241. Shah, A. R. et al. In vitro/ex vivo investigation of modified Utah electrode array to selectively sense and pace the sub-surface cardiac His bundle. *ACS Biomater. Sci. Eng.* **6**, 3335–3348 (2020).
242. Kang, Y. N., Chou, N., Jang, J. W., Choe, H. K. & Kim, S. A 3D flexible neural interface based on a microfluidic interconnection cable capable of chemical delivery. *Microsyst. Nanoeng.* **7**, 66 (2021).
243. Zhou, Y. et al. A silk-based self-adaptive flexible opto-electro neural probe. *Microsyst. Nanoeng.* **8**, 118 (2022).
244. Xia, M. et al. Scalable, flexible carbon fiber electrode thread arrays for three-dimensional probing of neurochemical activity in deep brain structures of rodents. *Biosens. Bioelectron.* **241**, 115625. https://doi.org/10.1016/j.bios.2023.115625 (2023).
245. Zhao, Q. et al. Highly stretchable and customizable microneedle electrode arrays for intramuscular electromyography. *Sci. Adv.* **10**, eadn7202. https://doi.org/10.1126/sciadv.adn7202 (2024).
246. Mueller, N. N. et al. Mechanically-adaptive, resveratrol-eluting neural probes for improved intracortical recording performance and stability. *npj Flex. Electron.* **9**, 64 (2025).
247. Seo, K. J. et al. A soft, high-density neuroelectronic array. *npj Flex. Electron.* **7**, 40 (2023).
248. Liu, J. et al. Ten-hour stable noninvasive brain-computer interface realized by semidry hydrogel-based electrodes. *Research* **2022**, 9830457. https://doi.org/10.34133/2022/9830457 (2022).
249. Ding, L. et al. Covalently bridging graphene edges for improving mechanical and electrical properties of fibers. *Nat. Commun.* **15**, 4880 (2024).
250. Long, G. et al. Carbon nanotube-based flexible high-speed circuits with sub-nanosecond stage delays. *Nat. Commun.* **13**, 6734 (2022).
251. Yuan, Y. et al. Ultra-high mobility transparent organic thin film transistors grown by an off-centre spin-coating method. *Nat. Commun.* **5**, 3005 (2014).
252. Gregory, B. A. et al. Structural and functional changes of deep layer pyramidal neurons surrounding microelectrode arrays implanted in rat motor cortex. *Acta Biomater.* **168**, 429–439 (2023).
253. Usoro, J. O. et al. Influence of implantation depth on the performance of intracortical probe recording sites. *Micromachines* **12**, 1158 (2021).
254. McNamara, I. N. et al. Electrode sharpness and insertion speed reduce tissue damage near high-density penetrating arrays. *J. Neural Eng.* **21**, 026030 (2024).
255. Chen, C. et al. Single-field evolution rule governs the dynamics of representational drift in mouse hippocampal dorsal CA1 region. *Adv. Sci.* **13**, e09532. https://doi.org/10.1002/advs.202509532 (2025).
256. Cornuéjols, R. et al. Flexible depth probes with PEDOT:PSS microelectrodes for chronic recording and stimulation. *ACS Appl. Mater. Interfaces* **17**, 42148–42161 (2025).
257. Liu, M.-G. et al. Acid-sensing ion channel 1a contributes to hippocampal LTP inducibility through multiple mechanisms. *Sci. Rep.* **6**, 23350. https://doi.org/10.1038/srep23350 (2016).
258. Cuellar, C. et al. Selective activation of the spinal cord with epidural electrical stimulation. *Brain Sci.* **14**, 650 (2024).
259. John, S. E. et al. Vascular remodeling in sheep implanted with endovascular neural interface. *J. Neural Eng.* **19**, 056018 (2022).
260. Qi, W. et al. Haemodynamics of stent-mounted neural interfaces in tapered and deformed blood vessels. *Sci. Rep.* **14**, 7212 (2024).
261. Li, Y. et al. Ultra-low frequency magnetic energy focusing for highly effective wireless powering of deep-tissue implantable electronic devices. *Natl. Sci. Rev.* **11**, nwae062. https://doi.org/10.1093/nsr/nwae062 (2024).
262. Boergens, K. M. et al. Laser ablation of the pia mater for insertion of high-density microelectrode arrays in a translational sheep model. Preprint at: https://doi.org/10.1088/1741-2552/ac0585 (2020).
263. Mestais, C. et al. Long-term sheep implantation of WIMAGINE®, a wireless 64-channel electrocorticogram recorder. *Front. Neurosci.* **13**, 847 (2019).
264. Cao, S. H. et al. Hand position fields of neurons in the premotor cortex of macaques during natural reaching. *Nat. Commun.* **16**, 3489 (2025).
265. Hu, K. et al. Decoding unconstrained arm movements in primates using high-density electrocorticography signals for brain-machine interface use. *Sci. Rep.* **8**, 10583. https://doi.org/10.1038/s41598-018-28940-7 (2018).
266. Li, W. et al. Multi-source domain adaptation for decoder calibration of intracortical brain-machine interface. *J. Neural Eng.* **17**, 066009 (2020).
267. Kuang, S., Morel, P. & Gail, A. Planning movements in visual and physical space in monkey posterior parietal cortex. *Cereb. Cortex* **26**, 731–747 (2016).
268. Gavrilov, N. & Nieder, A. Distinct neural networks for the volitional control of vocal and manual actions in the monkey homologue of Broca's area. *eLife* **10**, S.E62797 (2021).
269. Sponheim, C. et al. Longevity and reliability of chronic unit recordings using the Utah intracortical multi-electrode arrays. *J. Neural Eng.* **18**, 066044 (2021).
270. Card, N. S. et al. An accurate and rapidly calibrating speech neuroprosthesis. *N. Engl. J. Med.* **391**, 609–618 (2024).
271. Willett, F. R. et al. A high-performance speech neuroprosthesis. *Nature* **620**, 1031–1036 (2023).
272. Fang, H. & Yang, Y. Predictive neuromodulation of cingulo-frontal neural dynamics in major depressive disorder using a brain-computer interface system: a simulation study. *Front. Comput. Neurosci.* **17**, 1119685 (2023).
273. Holtzheimer, P. E. et al. Revisiting subcallosal cingulate deep brain stimulation for depression: long-term safety and effectiveness outcomes from a pooled analysis of 172 implanted patients. *Brain Stimul.* **18**, 1632–1640 (2025).
274. Wang, S.-J. et al. Organic bipolar transistors. *Nature* **606**, 700–705 (2022).
275. Iranmanesh, E. et al. Organic-inorganic hybrid piezotronic bipolar junction transistor for pressure sensing. *Microsyst. Nanoeng.* **10**, 80 (2024).

276. Shin, J. et al. Bioresorbable pressure sensors protected with thermally grown silicon dioxide for the monitoring of chronic diseases and healing processes. *Nat. Biomed. Eng.* **3**, 37–46 (2019).
277. Kim, H. et al. Motion artifact-controlled micro-brain sensors between hair follicles for persistent augmented reality brain-computer interfaces. *Proc. Natl. Acad. Sci. USA* **122**, e2419304122. https://doi.org/10.1073/pnas.2419304122 (2025).

Acknowledgements

This work is supported by the STI 2030-Major Project (2022ZD0209900), the National Natural Science Foundation of China (62574057, 62204057, 32471083, 82471276), Lingang Laboratory (LGL-8998-09), the National Key R& D Program of China (2021ZD0202805), the Innovative Research Team of High-level Local Universities in Shanghai, 111 Project (B18015) and we appreciate the support by Xiaomi Young Talents Program, Shanghai Municipal Science and Technology Major Project (2018SHZDZX01), ZJ Lab, Shanghai Center for Brain Science and Brain-Inspired Technology, and the young scientist project of MOE innovation platform.

Author contributions

Q.C., N.H. and C.T. contributed equally to this work. H.X., X.X. and E.S. conceived the study. Q.C., N.H. and H.X. performed the methodology. Q.C., N.H., C.T., P.L. and S.Q. conducted the investigation. Q.C., N.H. and C.T. prepared the figures. Q.C., N.H. and H.X. wrote the original draft. H.X., X.X. and E.S. reviewed and edited the manuscript. X.X. and E.S. supervised the work. E.S. acquired the funding. All authors approved the final manuscript.

Competing interests

The authors declare no competing interests.

Additional information

Correspondence and requests for materials should be addressed to Huize Xue, Xiao Xiao or Enming Song.